Articles in PresS. J Neurophysiol (May 22, 2013). doi:10.1152/jn.00961.2012

Fear signaling in the prelimbic-amygdala circuit: A computational modeling and recording study

Sandeep Pendyam[1†], Christian Bravo-Rivera[2], Anthony Burgos-Robles[2†], Francisco Sotres-Bayon[2†], Gregory J. Quirk[2], Satish S. Nair[1]

[1]Department of Electrical and Computer Engineering, University of Missouri, Columbia, MO;
[2]Departments of Psychiatry and Anatomy & Neurobiology, University of Puerto Rico School of Medicine, San Juan, PR

[†]Dr. Pendyam's present address: Qualcomm Technologies Inc, San Diego, CA
[†]Dr. Burgos-Robles's present address: MIT- McGovern Inst. for Brain Res., Cambridge, MA
[†]Dr. Sotres-Bayon's present address: Inst. de Fisiol. Cel.-Neurociencias, Univ. Nal. Aut. de México, Mexico.

Abbreviated title: The expression of fear response by mPFC-amygdala network.

Correspondence may be sent to:

Satish S. Nair, Ph.D.
Electrical and Computer Engineering
University of Missouri, Columbia, MO, 65211
Tel: 573-882-2964; Fax: 573-882-0397

Pages	31
Figures	9
Tables	6
Abstract	216 words

ABSTRACT

The acquisition and expression of conditioned fear depends on prefrontal-amygdala circuits. Auditory fear conditioning increases the tone responses of lateral amygdala (LA) neurons, but the increase is transient, lasting only a few hundred milliseconds after tone onset. It was recently reported that that the prelimbic (PL) prefrontal cortex transforms transient LA input into a sustained PL output, which could drive fear responses via projections to the lateral division of basal amygdala (BL). To explore the possible mechanisms involved in this transformation, we developed a large-scale biophysical model of the BL-PL network, consisting of 850 conductance-based Hodgkin-Huxley type cells, calcium-based learning, and neuromodulator effects. The model predicts that sustained firing in PL can be derived from BL-induced release of dopamine and norepinephrine that is maintained by PL-BL interconnections. These predictions were confirmed with physiological recordings from PL neurons during fear conditioning with the selective β-blocker propranolol and by inactivation of BL with muscimol. Our model suggests that PL has a higher bandwidth than BL, due to PL's decreased internal inhibition and lower spiking thresholds. It also suggests that variations in specific micro-circuits in the PL-BL interconnection can have a significant impact on the expression of fear, possibly explaining individual variability in fear responses. The human homologue of PL could thus be an effective target for anxiety disorders.

INTRODUCTION

The ability to respond appropriately to threatening stimuli is important for survival. The neural circuit that learns about such threats in the environment appears to be highly conserved across species. The amygdala, which receives convergent information about conditioned stimuli (CS; e.g., a tone) and unconditioned stimuli (US; e.g., a footshock), stores CS-US associations, and is thought to be a key element of this circuit. Electrophysiological studies have shown that the magnitude of tone responses in the lateral nucleus of the amygdala (LA) correlates with the acquisition and extinction of conditioned fear (Collins and Pare 2000; Quirk et al. 1995; Repa et al. 2001), consistent with a critical role of LA in generating fear responses.

There is a mismatch, however, between the duration of conditioned responses in LA neurons and the duration of conditioned freezing. Conditioned responses in LA last only a few hundred milliseconds after tone onset, and therefore cannot be solely responsible for maintaining freezing for tens of seconds. This suggests that additional structures are involved in the expression of conditioned fear. Burgos-Robles et al. (2009) showed that unit activity in the prelimbic (PL) region of the medial prefrontal cortex (mPFC) correlates with freezing, on a second to second basis, during a 30 second CS. Consistent with a role of PL in sustaining fear, pharmacological inactivation of PL reduces conditioned fear responses, whereas stimulation of PL enhances fear responses (Corcoran and Quirk 2007; Laurent and Westbrook 2008; Sierra-Mercado et al. 2011; Vidal-Gonzalez et al. 2006). Thus, PL activity seems to be vital for fear expression, but mechanisms that sustain PL tone responses are unknown.

PL receives inputs from the amygdala, hippocampus, thalamus and other cortical structures that are involved in fear conditioning (Gabbot et al. 2006; Vertes et al. 2004), and projects to lateral division of basal amygdala (BL), a region necessary for fear expression (Amano et al. 2011; Anglada-Figueroa and Quirk 2005; Herry et al. 2008; Laviolette et al. 2005). We developed a biophysical model of the BL-PL network consisting of 850 conductance-based Hodgkin-Huxley type cells, exhibiting the biophysical properties previously described for these neurons. In the model, BL receives input from LA, and projects to the central amygdala (Ce), which functions as the output station of the network, triggering freezing and release of neuromodulators. We implemented calcium-based synaptic plasticity, and neuromodulation with dopamine and norepinipherine, based on available *in vitro* data. We used this model to investigate the potential roles of several factors in sustaining PL tone responses including: (i) PL-BL network structure and connectivity, (ii) neuromodulators, and (iii) specific microcircuits within the PL-BL network. We then evaluated the extent to which the model agreed with existing and newly collected recording data.

METHODS

Single cell models

Conductance-based biophysical models were developed for principal cells and interneurons in the PL and BL structures, and in LA (input) and Ce (output) structures. All single cell models had two compartments, a soma and a dendrite.

PL cell model. Intrinsically bursting (IB) principal cells are the most common principal cell type in the deep layers of the rat mPFC (65%; Durstewitz et al. 2000; Yang et al. 1996), and they have previously been shown to participate in memory tasks (Fuster 1973). PL IB cells elicit a spike doublet followed by a train of spikes with spike frequency adaptation (Degenetais et al. 2002). PL interneurons are predominantly fast spiking inhibitory cells (Kawaguchi and Kubota, 1997). We modeled both these PL cells based on models in Durstewitz et al. (2000). The PL IB principal cell model had two compartments representing a soma (diameter of 21.8 μm; length of 28.6 μm), and an apical dendrite (diameter of 6.5 μm; length of 650 μm) (Durstewitz and Gabriel 2007). The specific membrane resistance, membrane capacitance and cytoplasmic (axial) resistivity were R_m=30 KΩ-cm^2, C_m=1.2 μF/cm^2, and R_a=150 Ω-cm, respectively (all within

ranges reported in Destexhe and Pare 1999; Spruston et al. 1994; Stuart and Spruston 1998). The leakage reversal potential (E_L) was set to -70 mV. The resulting V_{rest} was -66 mV (Durstewitz et al. 2000), with input resistance R_{IN} =164 MΩ (Durstewitz et al. 2000), and time constant $\tau_m = R_m C_m$=36 ms (Spruston et al. 1994). Both soma and dendritic compartments had the following currents: leak (I_L), spike-generating sodium current (I_{Na}), delayed rectifier potassium (I_{DR}), persistent sodium current (I_{Nap}), slowly inactivating potassium (I_D), inward rectifying potassium (I_{Kir}), high-voltage activated Ca^{2+} (I_{HVA}), and a calcium activated potassium (I_{KCa}) (Durstewitz et al. 2000). In addition, the dendrites had a hyperpolarization-activated cyclic nucleotide-gated current (I_{HCN})(Wang et al. 2002).

The PL interneuron model also had two compartments, a soma (dia 15 μm; length 15 μm) and a dendrite (dia 10 μm; length 150 μm). Each compartment contained fast Na^+ (I_{Na}) and delayed rectifier K^+ (I_{DR}) currents with kinetics (Durstewitz et al. 2000) that reproduced the much shorter spike duration that is characteristic of fast-spiking cells. The passive membrane properties were as follows: R_m=20 KΩ-cm^2, C_m=1.0 μF/cm^2, R_a=150 Ω-cm, and E_L=-70 mV (see appendix for mathematical details).

BL/LA cell model. Principal cells in the BLA (Basal, BA + Lateral, LA amygdala; shown to have similar properties) exhibit diverse firing properties in response to prolonged current injection, ranging from full frequency adaptation to firing repetitively (Faber et al. 2001). To represent different firing patterns, two major types of BL principal cells were modeled (Sah et al. 2003): type A with full adaptation and type B with medium adaptation. BL also contains local GABAergic interneurons (Woodruff and Sah 2007), which were modeled as fast spiking aspiny cells (Li et al. 2009). The parameter values for LA/BL cells were taken from our previous modeling study (Li et al. 2009). The BL/LA principal cell model had two compartments representing a soma (diameter 15 μm; length 15 μm) and a dominant apical dendrite (diameter 5 μm; length 400 μm) (Faber et al. 2001). The values for the specific membrane resistance, membrane capacity and cytoplasmic resistivity were R_m=30 KΩ-cm^2, C_m=1.0 μF/cm^2, and R_a=150 Ω-cm, respectively. The leakage reversal potential (E_L) was -75 mV. The resulting V_{rest} was – 69.5 mV, R_{IN} was ~150 MΩ, and $\tau_m = R_m C_m$ was 30 ms, all within the ranges previously reported (Faber et al. 2001; Washburn and Moises 1992). Both soma and dendritic compartments had the following currents: leak (I_L), spike-generating sodium (I_{Na}), delayed rectifier potassium (I_{DR}), persistent muscarinic (I_M), and high-voltage activated Ca^{2+} (I_{Ca}). In addition, the dendrite had the following currents: calcium-activated potassium (I_{KCa}), slow apamin-insensitive, voltage-independent afterhyperpolarization channel (I_{sAHP}), slowly inactivating voltage gated K^+ (I_D) and a hyperpolarization-activated channel (I_H) (Li et al. 2009). The interneuron model was the same as in PL.

Ce cell models. In our simplified Ce model, we used a late firing principal cell model for CeM cells (De Armentia and Sah, 2004; Dumont et al. 2002), with each having two compartments representing a soma (diameter of 15 μm; length of 15 μm) and a dominant apical dendrite (diameter of 5 μm; length of 300 μm) (details as in Li et al. 2011), with the following passive properties: R_m=30 KΩ-cm^2, C_m=1.0 μF/cm^2, R_a=150 Ω-cm, E_L=-60 mV for LF cell. Both soma and dendritic compartments had the following currents: leak (I_L), spike-generating sodium (I_{Na}), delayed rectifier potassium (I_{DR}), persistent muscarinic (I_M) and high-voltage activated Ca^{2+} (I_{Ca}). In addition to these, the dendrite had the following currents: calcium-activated potassium (I_{KCa}), slow apamin-insensitive voltage-independent after-hyperpolarization channel (I_{sAHP}), slowly

inactivating voltage-gated K^+ current (I_D) and hyperpolarization-activated channel (I_H) (same as in Li et al. 2011). For the CeL neurons, we used a modified version of the regular spiking CeM cell, with the same passive properties above, except for E_L which was -70 mV.

Neuromodulator effects

Neuromodulators are known to alter excitability of PL and BL cells during fear conditioning and extinction (Feenstra et al. 2001; Hugues et al. 2007; Myers and Davis 2007; Mueller et al. 2008). Although there are experimental reports related to effects of neuromodulation on cellular excitability for these regions (see below), and some evidence of co-activation and interaction between multiple neuromodulatory systems in general (Briand et al. 2007), the picture is not complete. The present model incorporated the effects of both dopamine (DA) and norepinephrine (NE) only. Conditioned fear stimuli modulate the activity of ventral tegmental area (VTA) DA neurons (Guarraci and Kapp, 1999), which in turn modulate fear and anxiety through ascending projections to PL, Ce, and the periaqueductal gray (Geisler et al. 2007). DA concentration is a critical determinant of D_1 versus D_2 signaling in mPFC (Trantham-Davidson et al. 2004), and in the amygdala in fear (Takahashi et al. 2010). Fear conditioned stimuli also evoke release of NE from locus coeruleus (LC) terminals into both mPFC (Hugues et al. 2007) and BLA (Galvez et al. 1996). Accordingly, we modeled NE effects via α- and β- type norepinephrine receptors. The neuromodulator receptors are activated differentially depending on NM levels (normalized concentration of neuromodulators, ranging from 0 to 1, determined by activity of Ce cells; see appendix). DA-D_1Rs, NE-βRs are activated at high concentrations (NM_H) while D_2Rs and NE- βRs are activated at all concentrations levels (NM_L, see appendix).

Dopaminergic modulation in PL. D_1 receptors in mPFC have been shown to affect cellular excitability in a number of ways. They shift the activation threshold of the persistent Na^+ current toward a more hyperpolarized potential, and slow inactivation (Durstewitz et al. 2000). We modeled this effect by shifting the activation threshold of the persistent Na^+ channel by (NM_H * -5 mV). D_1R activation has been shown to decrease persistent Na+ currents, affecting sEPSP amplitudes (Rotaru et al. 2007). The protein kinase A (PKA) pathway has been cited as a possible mechanism for action of D_1Rs on the persistent Na+ current (Sidiropolou et al. 2009). This was modeled by decreasing $g_{Nap,max}$ by 10*NM_H%. D_1R activation also reduces a slowly inactivating K^+ current in PFC principal cells (Durstewitz et al. 2000). This was modeled as a reduction in $g_{D,max}$ by 15*NM_H%. D_1 receptor activation reduces the half-width and amplitude of isolated dendritic Ca^{2+} spikes. This was modeled by reducing maximum HVA Ca^{2+} conductance ($g_{HVA,max}$) by 7*NM_H%. Stimulation of D_1 receptors have also been shown to increase the NMDA component of EPSCs by upto 30% over baseline in the PFC (Seamans et al. 2001). This was modeled by increasing $g_{NMDAA,max}$ by 20*NM_H. At low- DA, D_2R activation enhances $GABA_A$-like synaptic currents in the PFC, while decreasing non-NMDA or AMPA-like currents (Durstewitz et al. 2000). This was modeled by increasing $g_{GABA,max}$ by 40*NM_L% and decreasing $g_{AMPA,max}$ by 30*NM_L%.

Dopaminergic modulation in BL. Activation of DA D_1Rs decreases the spike threshold in BL cells by 3 mV and causes a 20-30% reduction in the slowly inactivating K^+ current (Kroner et al. 2004). These effects were modeled by shifting the activation curve of Na^+ channel by -1.5*NM_H mV and decreasing $g_{D,max}$ by 20*NM_H%. D_1R activation increases spontaneous inhibitory network activity (Loretan et al. 2004). This was modeled by increasing $g_{GABAA,max}$ for interneuron to principal cell synapses by 30*NM_H%. D_1R activation was reported to reduce NMDA current amplitudes by 20-30% in BL (Martina and Bergeron 2008). This effect was modeled by decreasing $g_{NMDA,max}$ by 20*NM_H % for connections between principal LAd cells. Activation of D_2 receptors enhances input resistance (Rosenkranz and Grace 2002), and this was modeled by

decreasing g_{leak} by 30*NM_L%.

Norepinephrine modulation in PL. Excitation of NE α2A-receptors reduces the concentration of cAMP, which in turn decreases hyperpolarization-activated cyclic nucleotide-gated (HCN) channel conductance (Wang et al. 2007; see appendix for details). This was modeled by reducing cAMP concentration by 30*NM_L%. NE α_2-receptor activation in the PFC caused a 3-5mV hyperpolarization in resting membrane potential (Carr et al. 2007). In addition, they also observed a significant increase in input resistance and increased number of evoked spikes. We modeled this by decreasing g_{leak} by 30*NM_L%. Stimulation of NE β receptors increases the NMDA-mediated Ca^{2+} current and the occurrence of spontaneous excitatory postsynaptic currents (Ji et al. 2008). Accordingly, the NMDA-mediated calcium influx was increased by 10*NM_H% on excitatory synaptic connections of PL cells that had β receptors. β_2-NE receptor activation has been shown to enhance firing and evoke Ca^{2+} dynamics in basal dendrites (Barth et al. 2007). This effect was modeled by a increasing g_{HVAmax} of dendritic Ca channels by 10*NM_H. In addition, systemic administration of the β-receptor antagonist propranolol has been reported to reduce both freezing (by 20-30%), and spontaneous activity (by 30%) in PL (Mueller et al. 2008; Rodriguez-Romaguera et al. 2009). Although such systemic administration may have other effects, we modeled it in two ways: (i) context-induced fear stress was modeled as causing tonic release of NE, independent of Ce, and independent of NM. This was modeled at the start of experiment by decreasing the maximum GABA conductance ($g_{GABAA,max}$) by 10%, and (ii) stress in high fear states (late conditioning and early extinction) caused phasic release of NE which was modeled by further decreasing $g_{GABAA,max}$ by (20*NM_H)%.

Norepinephrine modulation in BL. In BLA, NE- β inhibits the slow after-hyperpolarization that occurs after trains of action potentials, thereby facilitating spike firing (Tully and Bolshakov 2010). This was modeled by decreasing $g_{sAHP,max}$ by (10*NM_H)% in the presence of NE. NE β-R's activation also suppresses feedforward GABAergic inhibition of BLA projection neurons (Tully and Bolshakov 2010), which was modeled by reducing $g_{GABAA,max}$ by (10*NM_H)% . NE agonist (isoproterenol) enhances NMDA currents in BLA without affecting AMPA currents (Huang et al. 1998), and this effect was modeled by increasing $g_{NMDA,max}$ by (5*NM_H)%. Johnson et al. (2011) reported that NE decreases fEPSP (field excitatory post synaptic potential) amplitudes in the amygdala, whereas administration of selective NE-β agonists increased fEPSP amplitudes. From this, they concluded that NE-α receptors may increase the activity of inhibitory synapses, and this was also observed by Braga et al. (2004). We modeled this effect by increasing $g_{GABAA,max}$ by 10*NM_L% in interneuron to principal cells connections.

Since we use simplified modules for LA and Ce networks (as described in the next section), neuromodulator effects were not modeled in LA or Ce cells.

Network Architecture

Biological cell counts were used to generate a scaled-down (200:1; refs. in table) network model using the numbers shown in table 1. Connection strengths (weights) between cells need to be higher in such networks to compensate for the reduction in size (Dyhrfjeld-Johnsen et al. 2007). Our BL-PL network model had a total of 680 principal neurons (480 in PL and 200 in BL) and 170 GABAergic interneurons (120 in PL and 50 in BL). Input to this network was delivered from 24 LA cells, developed separately using our previous LA model (Li et al. 2009) modified to accommodate 30 sec tones (Burgos-Robles et al. 2009). We also included a simplified Ce model with eight GABAergic cells as the output station. Background input was delivered to all cells, in the form of random Poisson-distributed excitatory signals to match reported spontaneous firing rates in each region: PL: 5-7 Hz (Burgos-Robles et al. 2009), BL: 2-3 Hz (Herry et al. 2008), LA: 0.7-1.5 Hz (Quirk et al. 1995), and Ce: 1.8-2.8 Hz (Duvarci et al. 2011).

PL module. The PL module consisted of 320 principal cells in layer 2 and 160 principal cells in layer 5 (Fig. 1), reflecting the reported ratio of cells in these layers (Jones et al. 2005). Strong within-layer principal-principal cell connections exist in layers 2 and 5 (Jones et al. 2005; Markram et al. 1997). Connections between layers were modeled to match observations that ascending projections (layer 5 to layer 2) are more dense than descending projections (layer 2 to layer 5) (Fujisawa et al. 2008; Jones et al. 2005). Accordingly, 10% of layer 5 cells projected to layer 2 cells with source and target cells selected randomly. For connections between PL from BL cells, we used estimates from antidromic and orthodromic activation studies (Likhtik et al. 2005) which suggest that 32% of BL principal cells project to both layers 2 and 5 of PL (Orozco-Cabal et al. 2006).

BL module. The BL module included 200 principal cells modeled similar to those in LA (Li et al. 2009), with 130 fully adapting (type A) and 70 medium adapting (type B) cells (Sah et al. 2003), and had 50 interneurons. The interconnectivity within both BL and LA regions was sparse (1-5%; Samson and Pare 2005). Basal amygdala has dense bidirectional connectivity with the medial prefrontal cortex (mPFC; Gabbot et al. 2006). Electrical stimulation of the mPFC backfires a large proportion of BL projection cells (Likhtik et al. 2005) but does not elicit firing in Ce neurons (Quirk et al. 2003). This suggests that the BL contains a population of principal cells that project to mPFC but not to Ce, and another population that projects to Ce but not to mPFC (Popescu and Pare 2011). We therefore divided BL into two equal parts: BL1 (projecting to PL), and BL2 (receiving projections from PL). Because the projections from PL to BLA arise primarily from layer 2 (Likhtik et al. 2005), we connected a random 10% of PL layer 2 cells to BL2 cells.

LA module (Input). LA projects to BL, but does not receive feedback from either BL or PL. We used this fact to separate the LA module and provide it as 'input' to the rest of the model. This reduced model complexity and speeded up computations considerably. For this, we adapted our previous 10-cell LA model (Li et al. 2009; 8 principal cells+2 interneurons) for use with 30 sec tones. The adapted model was run ten times, with randomness in parameters such as connection strengths and background inputs. In the process a total of 80 principal cell model tone responses were created. LA is reported to have cells with varying tone responses (Quirk et al. 1995, 1997; Repa et al. 2001), and it is not presently clear which types project to BL (Pare and Durvaci 2012). Since the focus of the present study was to show how potentiated transient LA activity might be converted to sustained activity in PL, we specifically chose LA principal cell responses (from the 80 cells) that had tone responses whose z-scores (computed based on 10 bins prior to tone onset) dropped to less than 0.8 after 200 ms of the 30-sec tone onset (shown in results, Fig. 3A). This yielded a set of 24 principal cells that exhibited the cited transient conditioned responses. These cells were then projected to BL using a connectivity of 10% (Pitkanen et al. 1995), i.e., each LA cell projected to 10% of the BL cells (Table 2). We thus had a true transient input from LA, an assumption of the present study.

Ce module (Output). Similar to LA being the 'input' module for the model, Ce is the 'output' module, and essentially integrates tone responses of BL cells. That is, the role of Ce in our model was that of a simple integrator of activity in BL during the tone. In addition, the Ce module also received tone inputs, and if this activity exceeds a threshold, it resulted in neuromodulator release. We used a simplified module for the Ce region, with CeL and CeM sub-divisions. CeM receives direct projections from BL and indirect ones (via CeL) from LA (Pare and Duvarci 2012), and triggers neuromodulator release (via VTA and LC). This is consistent with reported Ce projections to LC (Bouret et al. 2003) and to VTA (Zahm et al. 1999) which release NE and DA, respectively. It has been estimated that ten percent of BL2 cells that receive input from PL cells also project to Ce (Likhtik et al. 2005). Ce cells also received non-plastic tone input (Linke et al. 2000; Pare et al. 2004; Ciocchi et al. 2010). The Ce module consisted of five CeM cells and two CeL cells, with inhibitory intrinsic connections. The CeM and CeL cell models were described in an earlier section. LA projects to CeL 'on' cells which then projects to CeL 'off' cells

(Ciocchi et al. 2010; Pare and Durvaci 2012) and the CeL 'off' cells project to CeM (Haubensak et al. 2010). In our simplified model we considered one each of CeL 'on' and 'off' cells. LA tone responses after conditioning acts via the CeL-on and CeL-off cells to reduce inhibition on CeM cells. Each CeM cell (total five) received six projections from randomly selected BL2 cells, and also received tone input.

The responses of these five CeM cells were then averaged by connecting them to a single regular spiking output cell (representing a downstream structure), and the response of this output cell determined neuromodulator release. Details of how Ce integrates all its inputs and controls neuromodulation is described in the Appendix section 'Neuromodulator release'. See appendix figure A2 for tone responses of the CeM output cell and neuromodulator concentration levels during the different phases of fear learning.

Distribution of neuromodulator receptors. We used biological estimates of DA receptors in mPFC (Santana et al. 2009), to distribute D_1 and D_2 receptors randomly on PL principal cells and interneurons in layers 2 and 5 (Table 3). Serotonergic and noradrenergic innervations have been reported to have similar densities and distributions, and are extremely widespread and largely overlapping (Sara 2009). Accordingly, we used estimates of serotonin receptors to populate NE receptors in PL (Santana et al. 2004). NE β-receptor subtypes are dispersed across all cortical layers (Goldman-Rakic et al. 1990), and so we used the random distributions of β-receptor subtypes in PL cells.

For BL, thirty percent of BLA principal cells have been reported to express NE receptors (Farb et al. 2010), while dopamine receptors have been shown to be present on upto 70% of BLA principal cells (Muller et al. 2009). Lacking biological information for the distribution of these neuromodulator receptors on interneurons, we iteratively determined and populated only principal cells with these receptors (Table 3).

Training protocol

The model training protocol of tone and shock inputs followed the unit recording study in Burgos-Robles et al. (2009), which included habituation, conditioning, and extinction phases. Each model tone lasted 30 sec and each shock lasted 500 ms, and the inter-tone interval was 60 sec. During the habituation phase, 5 tones were presented to the network to determine baseline tone responses. During the conditioning phase, 5 tones were paired with shocks delivered during the last 500 ms of each tone. During the extinction phase, 20 tones were delivered without any shock. We found that the weights did not change significantly during the gap between conditioning and extinction, and so modeled a gap of 180 sec, during which random background activity was present.

Simulations were performed on a Linux cluster, using pNEURON (Carnevale and Hines 2006), with the Crank-Nicholson integration method and an integration interval of 10 μs. To assess the robustness of the results, each model experiment was run with three different randomizations of intra- and inter-region network connectivity. This was done to avoid any preferential bias to particular input or network connectivity. All model results reported are averages over these three runs. The complete protocol was 48 mins long and required 7 hrs to run on a 40-node Linux cluster. Analysis of simulation output was performed using MATLAB.

To detect tone-elicited changes in PL activity, we divided the 30-sec tone into ten 3-sec bins. A z-score for each of these bins was calculated relative to ten pre-tone bins of equal durations. Each PL or BL cell was considered as tone responsive if the z-score of at least three bins exceeded 2.58, and these cells were selected for reporting the results.

Experimental Methods

Subjects. A total of 4 male Sprague-Dawley rats (Harlan Laboratories, Indianapolis, IN) weighing 270-320 g were housed and handled as described previously (Quirk et al 2000). Rats

were restricted to 18 g/day of standard laboratory rat pellets, followed by training to press a bar for food on a variable interval schedule of reinforcement (VI-30). Pressing a bar for food ensures a constant level of activity in which freezing can be reliably measured. All procedures were approved by the Institutional Animal Care and Use Committee of the University of Puerto Rico, School of Medicine in compliance with National Institutes of Health guidelines for the care and use of laboratory animals.

Surgery. After bar-press training, rats were anesthetized with intraperitoneal injections of a mixture of ketamine (80 mg/kg)-xylazine (10 mg/kg) and were stereotaxically implanted with an electrode microdrive in PL (+2.9mm AP; ±0.60mm ML; -2.6mm DV). Electrodes were fixed to the skull with dental cement and three stainless steel screws. After surgery, a triple antibiotic (Neosporin) was applied around the wound and an analgesic (Ketofen; 2 mg/kg) was injected intramuscularly. After surgery, animals were allowed to recover for 7 days before the experiments.

Histology. Upon completion of experiments, rats were transcardially perfused with 0.9% saline followed by 10% buffered formalin. Brains were extracted and stored in a 30% sucrose/ 10% formalin solution for several days. Coronal sections were cut (40 µm thick) in a cryostat, mounted on slides, and stained for Nissl bodies for cannula placement histology.

PL unit recording. Extracellular waveforms that exceeded a voltage threshold were digitized at 40 kHz and stored on a computer. Waveforms were recorded during pretone, tone, and post-tone periods, each lasting 30 s. Waveforms were then sorted offline using three-dimensional plots of principal component and voltage vectors (Offline Sorter; Plexon). Clusters formed by individual neurons were tracked across treatments. Timestamps of neural spiking and flags for the occurrence of tones and shocks were imported to NeuroExplorer for analysis (NEX Technologies). After conditioning, rats were tested for fear expression under a systemic injection of saline or β-receptor blocker (10mg/kg, i.p., 10 mins before testing). Two trials per test were averaged and examined for the detection of tone responses. To detect tone-elicited changes in PL activity, we divided the 30 s tone into 10 bins, each of 3 s duration. A *z*-score for each of these bins was calculated, relative to 5 pretone bins of equal duration. PL neurons were classified as showing excitatory tone responses if any two tone bins exceeded 2.58 *z*'s ($p < 0.01$, two-tailed). Furthermore, group peri-event time histograms were generated by averaging *z*-scores of all tone-responsive neurons. Comparisons across experimental phases were made using repeated-measures ANOVA.

Network parameters suggested by the model

Our network incorporated known parameters such as single cells responses, connectivity between PL and amygdala, interconnectivity in BLA and Ce, synaptic parameters, and information about neuromodulator receptor distribution. For parameters not available in the literature, we decided to optimize values to match experimental data related to spontaneous rates in PL and BL, and tone response profiles during the different phases of training, i.e., tone responses are higher and sustained only during high fear states (Burgos-Robles et al. 2009). The following optimized parameters thus constitute model predictions that await subsequent validation:

(i) *Initial weights and plasticity thresholds.* Each source cell randomly connected to X cells within the same layer, with a 'fan-out' X (# of target synapses) determined by an iterative process to achieve sustained activity in the BL-PL-Ce network (Table 2). The connectivity between PL (layer 2) and BL cells, and between LA and BL cells, was stronger (two-fold) compared to all other connections. Also, the plasticity thresholds for these connections were 20% lower compared to the other connections (see appendix, table A2).

(ii) *Fan-out in the network.* A network that showed sustained activity in PL cells required the following structure and connectivity (Fig. 1). The fan-out for BL-BL connections was 4, i.e., each

cell connected to 2% of the other principal cells randomly, suggesting that sparse connectivity is required for the observed spontaneous firing rate of 3 Hz in BL (Herry et al. 2008). As cited, BL had two populations of principal cells, BL1 (100 cells) which projected to PL, and BL2 (100 cells) which received projections from PL. LA projected randomly to both these BL cell populations with a fan-out of 20. The recurrent connectivity between BL and PL was modeled as follows: Thirty percent of BL1 principal cells projected to principal cells in PL layers 5 and 2, with fan-outs of 5 and 2, respectively. The connectivity within each of the PL layers 2 and 5 was 3%, which suggests that higher within-region connectivity (compared to BL) is needed for reproducing the higher experimental spontaneous firing rates (5-7 Hz; Burgos-Robles et al. 2009). Ten percent of PL layer 5 cells projected to PL layer 2 cells. This additional connectivity between PL layers 5 and 2 introduced delays in the network and helped extend the activity of PL and BL cells. To complete the loop, 10% of PL layer 2 cells projected to BL2 cells with a fan-out of 2. The fan-out numbers used were iteratively determined to match experimental data, including spontaneous firing rates, and activity in the BL-PL network (e.g., Burgos-Robles et al. 2009).

(iii) *Neuromodulator effects* – As cited, we modeled the effects of DA and NE, and given recent evidence of co-activation and interaction between multiple neuromodulatory systems (Briand et al. 2007), assumed that other neuromodulator effects, if any, would be via the same pathways as for these two. Since data about neuromodulator effects are typically reported as increasing or decreasing either intrinsic or synaptic excitability, without precise (e.g., in vitro only) quantification, we iteratively quantified the effects to match experimental data. We note that, by themselves, different combinations of the two parameter sets above (initial weights and plasticity thresholds, or fan-out) failed to provide the pattern of sustained tone responses seen experimentally (Burgos-Robles et al. 2009), leading to conclusion that differences in the levels of neuromodulation between low and high fear states might be involved. Accordingly, we iterated on neuromodulator effects to match the pattern of tone responses during the training protocol.

RESULTS

In vitro firing properties

Single neurons in the model exhibited reported *in vitro* firing properties. In response to injected current, model PL cells exhibited the spiking behavior of IB prefrontal neurons, eliciting a spike doublet followed by a train of spikes showing rate adaptation (Fig. 2A) (Durstewitz et al. 2000; Degenetais et al. 2002). The PL interneuron model reproduced the experimentally observed non-adapting repetitive firing behavior of fast spiking cells (Lang and Pare 1998; Woodfruff and Sah 2007). BL model cell responses to current injections also matched experimental data reported in Faber et al. (2001). For instance, in response to a depolarizing current step (400 pA 600 ms), type A neurons fired only 3 spikes (Fig. 2B), and type B neurons fired 9 spikes before adapting. A hyperpolarizing current initiated a slow depolarizing sag (right panel in Fig. 2B), due to the activation of I_H (Womble and Moises 1993).

Recording studies have shown significant differences in passive properties between PL and BL cells. Indeed, PL principal cells exhibit spike thresholds in the range of -51 ± 5 mV (Degenetais et al. 2002), while BL cells are much lower at -41 ± 1 mV (Faber et al. 2001). Consistent with this, the average firing rate for PL cells is 5-7 Hz (Burgos-Robles et al. 2009) compared to 2-3 Hz for BL cells (Herry et al. 2008). Because neuromodulators affect intrinsic excitability of cells, they could further amplify the differences between PL and BL responses. The behavioral consequences of such differences are discussed later.

Sustained conditioned tone responses in the PL-BL network

LA neurons show conditioned tone responses that are transient and have a short-latency to tone onset (12 ms) (Quirk et al. 1995, 1997; Repa et al. 2001). In contrast, PL cells show a longer latency response (> 90 ms) and the response last the duration of the tone (Burgos-Robles et al. 2009). Figure 3A shows the tone responses of a sample cell during habituation and early extinction phases. The sustained activity is clearly seen during tone in the early extinction trial and lasts 3-6 sec after tone offset. Figure 3B shows the peri-event time histograms (PETHs) of model tone responses (bin width 3 sec; tone duration 30 sec) of LA, BL, PL cells, which matched published findings. Averages were taken over two trials for each phase: habituation (trials 4-5), conditioning (trials 4-5), early extinction (trials 1-2), and late extinction (trails 19-20). The percentage of cells showing sustained conditioned tone responses in both BL and PL also matched experimental reports, BL model: 37% (75/200) compared with 33% (Amano et al. 2011); PL model: 26% (127/480) compared with 23% (Burgos-Robles et al. 2009). The tone responses of the remaining 63% of BL cells and 74% of PL cells were not significantly different to average pre-tone (duration of 30 sec) responses. The spontaneous firing rates (measured 60 sec after conditioning) of the non-tone responsive cells were also similar to those of the tone responsive cells. The sustained tone responsive cells in BL belonged to the BL2 population that received projections from PL. In PL, the sustained tone responsive cells were equally represented in both layers 2 and 5. Even with tone lasting 20s or 40s, responses of model PL cells were found to last the entire duration of the tone, and persisted for 3-6 s after tone offset. Thus, the model was able to convert transient LA activity to sustained tone responses in PL cells. See Figure A2 in appendix for tone responses of Ce cells that result in neuromodulator release.

Mechanisms necessary for sustaining tone responses in PL and BL cells

Previous studies have shown that post-conditioning lesions of BL eliminate conditioned freezing (Anglada-Figueroa and Quirk 2005). Also, pharmacological inactivation of BL blocks expression of conditioned fear (Falls et al. 1992; Herry et al. 2006; Sierra-Mercado et al. 2011; Amano et al. 2011). Furthermore, pharmacological inactivation of BL eliminates fear conditioned olfactory responses in PL neurons (Laviolette et al. 2005). This suggests that BL provides a critical tone input to PL. Consistent with these experimental reports, we found in the model that inactivation of LA or BL, or blocking neuromodulators, eliminated sustained model tone responses in PL (Fig. 4A). We then selectively inactivated projections from BL to PL, without altering PL to BL projections. This caused a minor change in average z-scores for PL cells (< 8% reduction) and in the number of tone responsive PL cells (< 3% reduction).

Figure 4B shows that LA inactivation completely eliminated tone responses in BL. Also, PL inactivation resulted in a 73% decrease in BL tone responses (average z-scores; Fig. 4B, right panel), and a 78% decrease in the tone responsive BL cells (#TR cells = 9 of 75) that showed sustained activity. These results are consistent with the >50% reduction in freezing observed experimentally after post conditioning inactivation of PL (Sierra-Mercado et al. 2011). Similarly for PL, inactivating BL to PL projections caused a minor change in average z-scores for BL cells (see Fig. A3).

Blocking neuromodulator release (Fig. 4, left panels) in the model caused a pronounced decrease in average sustained tone responses in both PL (83%) and BL (85%). The percentage of cells with sustained tone responses also decreased, by 93% in PL (#TR cells = 9 of 127), and by 90% in BL (#TR cells = 8 of 75). These results are in agreement with behavioral reports that show a 65% decrease in freezing after systemic administration of NE antagonist propranolol (Rodriguez-Romaguera et al. 2009).

As expected, LA inactivation eliminated short-latency tone responses in BL and PL (Fig. 4). Similarly, BL inactivation also eliminated short-latency PL tone responses. With blockade of neuromodulator release (equivalent to lesioning Ce), short-latency tone responses were still

observed in BL and PL, however, no cells could sustain tone responses beyond two bins (> 3s). Then, we selectively turned off connectivity from BL to PL, and this resulted in a 7% decrease in tone responses of PL and BL cells (see Fig. A3). The percentage of cells with sustained tone responses also decreased, by 7% in PL (#TR cells = 118 of 127), and by 10% in BL (#TR cells = 66 of 75).

In contrast to tone responses, inactivations had modest effects on spontaneous activity (Fig. 4, right panels; recorded between conditioning and extinction). BL inactivation reduced spontaneous firing rates in PL cells by 27%, from 5.2 to 3.8 Hz. Also, blocking neuromodulators (both phasic and tonic) decreased the spontaneous activity in PL by 23%, from 5.2 to 4.1 Hz, consistent with the experimentally observed reductions seen with systemic propranolol (Rodriguez-Romaguera et al. 2009). Inactivation of PL had a larger effect on spontaneous firing rates in BL cells, dropping the average by 48%, from 3.1 to 1.6 Hz. Also, blocking neuromodulators (both phasic and tonic release) decreased the spontaneous activity in BL by 20%, from 3.1 to 2.5 Hz. Furthermore, inactivation of LA reduced spontaneous firing rates in model BL cells by 10%, from 3.1 to 2.8 Hz. The effect of inactivation on tone responses was larger than on spontaneous activity because of increased phasic activity during the tone. The factors that contributed to this phasic activity were potentiated LA tone responses, leading to neuromodulator release and to increased PL-BL-Ce activity.

Experimental validation of model predictions

Model inactivation experiments (Fig. 4) predict that blockade of neuromodulator release and inactivation of BL will both eliminate sustained PL tone responses. Inactivating β-NE receptors in the model in order to match propranolol (selective β-receptor blocker) administration experiments reduced the number of model tone responsive PL cells by 80% (#TR cells = 23 of 115) and reduced average z-scores by 85% (see Fig. 5A; top panel). To test this prediction, we recorded from PL neurons in rats subjected to auditory fear conditioning. Indeed, systemic propranolol administration (see Fig. 5A; bottom panel) completely abolished sustained tone responses in PL cells (ANOVA with repeated measures: $F_{(1,12)}$=7.88, p= 0.016).

Also consistent with model findings, inactivation of BL with muscimol eliminated sustained activity in actual PL cells. Figure 5B shows PSTH's of average tone responses of PL cells before and after BL inactivation for the model (top panel) and experiments (from Sotres-Bayon et al. 2012; bottom panel). Model experiments also suggested that sustained tone responses in BL cells were necessary for sustained activity in PL cells. Although this prediction has not yet been experimentally validated, a recent study (Amano et al. 2011) does support our finding that BL neurons exhibit sustained tone responses during the expression of fear.

Perturbation studies reveal the importance of microcircuits in sustaining tone responses

In addition to gross manipulations of model connectivity, we were also interested in how manipulations of fine network connectivity might affect sustained firing. These included the % source cells that project to BL from PL and vice versa, as well as the distribution of neurotransmitter receptors in each region. For our optimized model (control case), these parameters were as follows: In the BL1 cluster, a random 40% of BL1 cells received inputs from LA, and a random 48% BL1 cells expressed at least one type of neuromodulator receptors. In the BL2 cluster, 40% of BL2 cells received inputs from LA, and 50% of BL2 cells expressed neuromodulator receptors. About 60% of the PL layer 2 cells projecting to BL2 expressed neuromodulator receptors and 50% of BL1 cells projecting to PL layers 2 and 5 expressed neuromodulator receptors. Finally, a random 30% of BL2 cells projected to Ce.

The parameters cited above determine the structure of the pertinent microcircuits between PL and BL regions. We varied these parameters to determine their relative contributions to tone responses. Compared to the optimized model (Table 2), a 10% increase or decrease in the number of source cells in the BL1 to PL projection resulted in no significant changes in

sustained tone responses or in spontaneous activity of BL and PL cells (Table 4a). However, increasing the number of source cells in the PL to BL2 projection by +10% increased the tone responsiveness of BL and PL cells, while decreasing this number by -10% decreased their tone responsiveness (Table 4a). This shows that PL to BL connections can have a much larger impact on sustained activity in PL-BL network than the BL to PL connections (see Fig. A3).

Significant changes in PL-BL tone responses were also observed when connections were further classified based on projecting cells expressing neuromodulator receptors. For example, increasing (from 25% to 100%) the percentage of source BL cells expressing neuromodulator receptors projecting to target PL cells had no significant effect on PL tone responses (Table 4b). However, increasing (by the same amount) the percentage of source PL cells expressing neuromodulator receptors projecting to target BL cells increased the average z-scores for BL cells from 2.9 to 3.9, and for PL cells from 3.3 to 4.4 (Table 4b). Thus, PL has a larger influence on BL than the other way round, perhaps stemming from the higher spontaneous firing rate of PL (5.1 Hz) compared to BL (2.9 Hz) model cells. This implies that microcircuits with specific connectivity and neuromodulator receptor distributions are required for sustained activity.

Generation of sustained conditioned tone responses in PL involves multiple structures

In summary, based on inactivation and perturbation studies, transient LA tone responses relayed to Ce via BL are insufficient to generate sustained activity in the PL-BL network. However, with neuromodulator release, tone inputs to Ce, and recurrent PL-BL connections, the same LA inputs resulted in sustained PL tone responses (Fig. 6) as follows: Increased LA activity during late conditioning and early extinction (trials 3-5 of conditioning and 1-3 of extinction; > 3-5 spikes per 200 ms from LA) triggers neuromodulator release into PL increasing tone responses in PL. This activity in PL was then relayed to Ce via BL, thereby sustaining neuromodulator release into the PL-BL network. Also, tone inputs to Ce, in addition to PL-induced BL activity, were required to increase Ce activity above threshold. After tone offset, the diminished drive from Ce could not sustain neuromodulator release, causing PL tone responses to gradually decrease in 5-6 sec. For the same reason, shock-induced neuromodulator release could not be sustained in the absence of tone inputs to Ce.

Limitations. Our model has a number of limitations: 1) The model was scaled 1/200 in cell numbers to permit reasonable simulation times. Future studies could test whether the qualitative conclusions and predictions hold for larger models. 2) The release of neuromodulators in the model was assumed to be a function of Ce activity (freezing), with the amount of release being proportional to Ce activity. More experiments are required to validate the assumed correlation between Ce activity and neuromodulator release in PL, as well as in quantifying the effects of neuromodulators, including interactions, particularly at physiological levels in vivo. 3) The role of inputs from other regions in sustaining PL tone responses, such as the hippocampus, is not known and was not modeled.

DISCUSSION

Auditory fear conditioning results in sustained conditioned tone responses in PL that are correlated with freezing on a second to second basis (Burgos-Robles et al. 2009). We developed a computational network model of LA, BL and PL regions using biological data, to shed light on how this LA-BL-PL circuit might convert transient LA tone responses to sustained conditioned tone responses in PL.

Cortex codes 'intensity', amygdala codes 'valence'

Neurons in amygdala and prefrontal cortex encode multiple cognitive and emotional saliencies, and the interconnections between these structures are crucial for emotional behavior in both animals and humans (Salzman and Fusi 2010; Kim et al. 2011). Our findings related to the role of the PL-BL network in the expression of fear are consistent with these reports. Using a theoretical model, Salzman and Fusi (2010) suggest that emotions can be characterized along two axes, 'valence' (pleasant versus unpleasant) and 'intensity' (or arousal). During fear conditioning, BLA provides the 'valence,' after a few trials of fear conditioning, in the form of unpleasantness due to tone associated with shock, and PL provides the 'intensity' for this emotional state (freezing during tone).

Specifically, PL receives stimulus-related input from BLA (Gabbott et al. 2006), and freezing triggers the release of neuromodulators into PL (Hughes et al. 2007). Our model experiments indicate that PL can integrate these two influences and sustain tone responses after fear conditioning as follows (see Fig. 6): During early conditioning, tone responses in BLA cannot elicit fear responses ('valence' is still ambiguous). As conditioning progresses, BL receives potentiated (transient) tone responses from LA (signaling unpleasantness) and transfers them simultaneously to PL, and to Ce. This causes CeM activity to increase, eliciting fear and freezing via projections to downstream structures such as the periaqueductal gray. Fear results in the release of neuromodulators such as dopamine and norepinephrine into PL and BLA (Geisler et al. 2007; Guarraci and Kapp 1999), increasing the excitability of PL and BL cells. Recurrent connectivity between PL and BL further increases tone-related activity in both structures thereby increasing the duration of freezing by sustained activity in both regions. Thus, PL plays a key role in increasing the 'intensity' of the emotional state.

We performed parametric studies varying synaptic weights, thresholds of synaptic plasticity, percentage connectivity, and distributions of neuromodulator receptors in BL and PL cells. These experiments revealed that the most critical factor for sustaining PL tone responses was activity in BL leading to neuromodulator release. In contrast, the most important mechanism for sustaining BL tone responses was network connectivity from PL (layer 2) to the BL cell cluster (BL2) that projects to Ce. *The model thus revealed how the various structures and mechanisms act in concert to sustain conditioned PL tone responses, and provided insights into their relative contributions.*

Neuromodulator release, rather than BL input, sustains PL tone responses

In the model, two pathways convey potentiated LA tone responses to PL. One is through direct ascending projections from BL to PL. The other is via an indirect pathway from BL to CeM, triggering neuromodulator release in PL. Because LA responses are transient, maintaining PL responses for the duration of the tone would require either continuous excitation via the bidirectional PL-BL loop, or continuous neuromodulator release into PL. Model experiments varying fan-out and connection strengths alone revealed that the bidirectional BL-PL connections were not sufficient, i.e., activity in PL was either too high (>15 Hz), or oscillatory, and PL responses continued long beyond tone offset. Adding the effects of neuromodulation in PL and BL revealed that the model was able to replicate biological data only with weak BL-PL and strong PL-BL connections. We then selectively turned off the BL to PL connectivity and found that the PL tone responses dropped about 5%, but continued to be

sustained. This important observation suggests that it is neuromodulator release into PL and not direct excitation from BL that sustains tone responses in PL. *The model thus makes a testable prediction that inactivating projections from BL to PL would not eliminate sustained tone responses in PL.* This could be experimentally verified by selectively inactivating BL axons to PL during tone delivery, using optogenetic techniques.

Neuromodulators sustain activity in PL after tone offset

Conditioned tone responses in PL are sustained for several seconds following tone offset (Burgos-Robles et al. 2009). In the model, strong LA transient responses generated strong BL responses, leading to phasic neuromodulator release. The increase in PL and BL activity during conditioned tones caused additional sustained neuromodulator release via a positive feedback loop. As discussed earlier, tone inputs to Ce cells contributed to neuromodulator release in the model only in the presence of potentiated LA or BL inputs. After tone offset, the absence of tone inputs to Ce caused a drop in Ce activity. This drop led to a gradual (not immediate) decrease in neuromodulator release due to the positive feedback loop, allowing persistence of activity in PL for up to 6 sec. This same mechanism sustained tone responses in BL past tone offset, in agreement with a recent report (Amano et al. 2011). In partial support of this mechanism, microdialysis studies show that neuromodulator concentration levels are elevated in the extracellular mPFC even after the cessation of conditioning and extinction training (Hugues et al. 2007).

Activity in BL relays sustained activity in PL to Ce

PL tone responses have to be relayed to Ce to elicit sustained freezing during the tone. Model experiments suggest that this is accomplished via the PL to BL to Ce pathway. This leads to the prediction that a population of BL cells (BL2 cells in our model) would exhibit sustained activity during conditioned tones. Partial validation for this was provided by a recent report that showed 15% of cells in BL exhibited sustained responses throughout the duration of a 20 sec tone (Amano et al. 2011). The model also showed that inactivation of BL completely eliminated conditioned responses in PL, consistent with our recent experimental data (see results, Fig. 5B). Furthermore, inactivation of PL reduced activity in model BL cells by 50%, also matching experimental results which show a 60% decrease in freezing with inactivation of PL (Sierra-Mercado et al. 2011). *Thus, sustained activity in BL is also necessary for converting a transient LA input into sustained expression of fear, by increasing Ce activity beyond a threshold level.*

Specific PL-BL microcircuits modulate fear expression

Although interactions between the amygdala and the medial prefrontal cortex (mPFC) have been shown to be critical for emotional processing in both animals and humans (Salzman and Fusi 2010; Kim et al. 2011), the relative roles of the two projections are unknown. The model was used to assess the relative importance of PL to BL and BL to PL projections during the expression of fear. The projections from PL to BL affect sustained tone responses more than vice versa: (i) increasing the number of PL cells connected to BL had a more pronounced impact on activity in BL, compared to increasing the number of BL cells projecting to PL, and (ii) microcircuits where PL cells with neuromodulator receptors projected to BL influenced activity in BL significantly more than similar projections from BL to PL. PL thus plays a dominant role in controlling the expression of fear via projections to BL. This is because PL principal cells have higher spike thresholds compared to BL cells. The minor influence of BL on PL observed in model experiments is also consistent with the experimental observation that very few PL cells (<10%) were tone responsive during habituation (Burgos-Robles et al. 2009). *Thus, differences in cellular properties and local connectivity endow PL with a higher bandwidth that is important for modulating BL tone responses.*

As noted by Sotres-Bayon and Quirk (2010), PL receives various inputs such as the emotional history of a stimulus (via amygdala), context and time (via hippocampus), internal state (via brainstem monoamines), and cognitive-mnemonic information (via orbital and lateral PFC). In contrast, the amygdala may not receive higher order cognitive information. *Thus, the higher bandwidth provides PL with flexibility in integrating this information, and determining appropriate responses to danger* cues.

CONCLUSIONS

A biophysical BL-PL network model incorporating known conductances, connectivity, and plasticity mechanisms, provided insights into the mechanisms responsible for generating sustained tone responses in PL. Model experiments suggest that fear-induced neuromodulator release in PL, and recurrent connections between BL and PL, were the key contributors to sustaining conditioned tone responses in PL. At the translational level, these model experiments suggest that individual variability in fear responses may be due to differences in connectivity in the PL to BL2 microcircuit. The network model will next be expanded to include other relevant regions with the long term goal of gaining insights into pathologies associated with the fear circuit, e.g., post traumatic stress disorder.

Acknowledgments

This research was supported in part by National Institutes of Mental Health Grants R01-MH087755 to SSN, and R01-MH058883 and R01-MH081975 to GJQ.

REFERENCES

Amano T, Duvarci S, Popa D, Pare D. The fear circuit revisited: contributions of the basal amygdala nuclei to conditioned fear. *J Neurosci* 31:15481-15489, 2011.

Anglada-Figueroa D, Quirk GJ. Lesions of the basal amygdala block expression of conditioned fear but not extinction. *J Neurosci* 25:9680-9685, 2005.

Barth AMl, Vizi ES, Lendvai B. Noradrenergic enhancement of Ca2+ responses of basal dendrites in layer 5 pyramidal neurons of the prefrontal cortex. *Neurochem Int* 51:323-327, 2007.

Bernardi RE, Lattal KM. A role for a1-adrenergic receptors in extinction of conditioned fear and cocaine conditioned place preference. *Behav Neurosci* 124: 204–210, 2010.

Bouret S, Duvel A, Onat S, Sara SJ. Phasic activation of locus ceruleus neurons by the central nucleus of the amygdala. *J Neurosci* 23: 3491–3497, 2003.

Braga MFM, Aroniadou-Anderjaska V, Manion ST, Hough CJ, Li H. Stress Impairs α1A Adrenoceptor-Mediated Noradrenergic Facilitation of GABAergic Transmission in the Basolateral Amygdala. *Neuropsychopharmacology* 29:45-58, 2004.

Briand LA, Gritton H,Howe WM, Young DA,Sarter M. Modulators in concert for cognition: modulator interactions in the prefrontal cortex. *Prog Neurobiol* 83:69–91, 2007.

Burgos-Robles A, Vidal-Gonzalez I, Quirk GJ. Sustained conditioned responses in prelimbic prefrontal neurons are correlated with fear expression and extinction failure. *J Neurosci* 29: 8474-8482, 2009.

Byrne JH, Roberts JL. *From Molecules to Networks – An introduction to cellular and molecular neuroscience*. Elsevier Academic Press, 2004.

Carnevale NT, Hines ML. *The NEURON Book*. Cambridge, UK: Cambridge University Press, 2006.

Carr DB, Andrews GD, Glen WB, Lavin A. α2-Noradrenergic receptors activation enhances excitability and synaptic integration in rat prefrontal cortex pyramidal neurons via inhibition of HCN currents. *J Physiol* 584:437-450, 2007.

Ciocchi S, Herry C, Grenier F, Wolff SB, Letzkus JJ, Vlachos I, Ehrlich I, Sprengel R, Deisseroth K, Stadler MB, Muller C, Luthi A. Encoding of conditioned fear in central amygdala inhibitory circuits. *Nature* 468:277-282, 2010.

Corcoran KA, Quirk GJ. Activity in prelimbic cortex is necessary for the expression of learned, but not innate, fears. *J Neurosci* 27: 840-844, 2007.

Collins DR, Paré D. Differential fear conditioning induces reciprocal changes in the sensory responses of lateral amygdala neurons to the CS(+) and CS(-). Learn Mem 7: 97-103, 2000.

De Armentia ML, Sah P. Firing properties and connectivity of neurons in the rat lateral central nucleus of the amygdala. *J Neurophysiol* 92: 1285-1294, 2004.

Degenetais E, Thierry AM, Glowinski J, Gioanni Y. Electrophysiological properties of pyramidal neurons in the rat prefrontal cortex: an in vivo intracellular recording study. *Cereb Cortex* 12: 1-16, 2002.

Destexhe A, Pare D. Impact of network activity on the integrative properties of neocortical pyramidal neurons in vivo. *J Neurophysiol* 81:1531–1547, 1999.

Durstewitz D, Seamans JK, Sejnowski TJ. Dopamine-mediated stabilization of delay-period activity in a network model of prefrontal cortex. *J Neurophysiol* 83: 1733-1750, 2000.

Durstewitz D, Gabriel T. Dynamical basis of irregular spiking in NMDA-driven prefrontal cortex neurons. *Cereb Cortex* 17:894-908, 2007.

Dumont É, Martina M, Samson R, Drolet G, Pare D. Physiological properties of central amygdala neurons: species differences. *Eur J Neurosci* 15:545-552, 2002.

Duvarci S, Popa D, Pare D. Central amygdala activity during fear conditioning. *J Neurosci* 31: 289–294, 2011.

Dyhrfjeld-Johnsen J, Santhakumar V, Morgan RJ, Huerta R, Tsimring L, Soltesz I. Topological determinants of epileptogenesis in large-scale structural and functional models of the dentate gyrus derived from experimental data. *J Neurophysiol* 97:1566-1587, 2007.

Faber ESL, Callister RJ, Sah P. Morphological and electrophysiological properties of principal neurons in the rat lateral amygdala in vitro. *J Neurophysiol* 85:714-723, 2001.

Falls WA, Miserendino MJ, Davis M. Extinction of fear potentiated startle: blockade by infusion of an NMDA antagonist into the amygdala. *J Neurosci* 12:854–863, 1992.

Farb C, Chang W, LeDoux JE. Ultrastructural characterization of noradrenergic axons and beta-adrenergic receptors in the lateral nucleus of the amygdale. *Front Behav Neurosci* 4:162, 2010.

Feenstra MG, Vogel M, Botterblom MH, Joosten RN, de Bruin JP. Dopamine and noradrenaline efflux in the rat prefrontal cortex after classical aversive conditioning to an auditory cue. *Eur J Neurosci* 13:1051-1054, 2001.

Fujisawa S, Amarsingham A, Harrison MT, Buzsaki G. Behavior-dependent short-term assembly dynamics in medial prefrontal cortex*. Nat Neurosci* 11:823-833, 2008.

Fuster JM. Unit activity in prefrontal cortex during delayed-response performance: neuronal correlates of transient memory. *J Neurophysiol* 36:61–78, 1973.

Gabbott PL, Warner TA, Busby SJ. Amygdala input monosynaptically innervates parvalbumin immunoreactive local circuit neurons in rat medial prefrontal cortex. *Neuroscience* 139:1039-1048, 2006.

Gabbott PL, Warner TA, Jays PRL, Salway P, Busby SJ. Prefrontal cortex in the rat: projections to subcortical autonomic, motor, and limbic centers. *J Comp Neurol* 492:145-177, 2005.

Gaiarsa JL, Caillard O, Ben-Ari Y. Long-term plasticity at GABAergic and glycinergic synapses: mechanisms and functional significance. *Trends Neurosci* 25: 564–570, 2002.

Galvez R, Mesches MH, McGaugh JL. Norepinephrine release in the amygdala in response to footshock stimulation. *Neurobiol Learn Mem* 66:253–257, 1996.

Geisler S, Derst C, Veh RW, Zahm DS. Glutamatergic afferents of the ventral tegmental area in the rat. *J Neurosci* 27:5730-5743, 2007.

Gerstner W, Kistler W. *Spiking neuron models: Single neurons, populations, plasticity*. Cambridge University Press, 2002.

Goldman-Rakic PS, Lidow MS, Gallager DW. Overlap of dopaminergic,adrenergic, and serotonergic receptors and complementarity of their subtypes in primate prefrontal cortex. *J Neurosci* 10:2125-2138, 1990.

Guarraci FA, Kapp BS. An electrophysiological characterization of ventral tegmental area dopaminergic neurons during differential Pavlovian fear conditioning in the awake rabbit. *Behav Brain Res* 99:169-179, 1999.

Haubensak W, Kunwar PS, Cai H, Ciocchi S, Wall NR Ponnusamy R, Biag J, Dong HW, Deisseroth K, Callaway EM, Fanselow MS, Luthi A, Anderson DJ. Genetic dissection of an amygdala microcircuit that gates conditioned fear. *Nature* 468:270–76, 2010.

Herry C, Trifilieff P, Micheau J, Luthi A, Mons N. Extinction of auditory fear conditioning requires MAPK/ERK activation in the basolateral amygdala. *Eur J Neurosci* 24: 261–269, 2006.

Herry C, Ciocchi S, Senn V, Demmou L, Muller C, Luthi A. Switching on and off fear by distinct neuronal circuits. *Nature* 454:600-606, 2008.

Huang CC, Lin CH, Gean PW. Potentiation of N-methyl-D-aspartate currents by isoproterenol in the acutely dissociated rat amygdalar neurons. *Neurosci Lett* 253:9–12, 1998.

Hugues S, Garcia R, Lena I. Time course of extracellular catecholamine and glutamate levels in the rat medial prefrontal cortex during and after extinction of conditioned fear. *Synapse* 61:933-937, 2007.

Jones BF, Groenewegena HJ, Witter MP. Intrinsic connections of the cingulate cortex in the rat suggest the existence of multiple functionally segregated networks. *Neuroscience* 133:193-207, 2005.
Ji XH, Cao XH, Zhang CL, Feng ZJ, Zhang XH, Ma L, Li BM. Pre- and postsynaptic beta-adrenergic activation enhances excitatory synaptic transmission in layer V/VI pyramidal neurons of the medial prefrontal cortex of rats. *Cereb Cortex* 18:1506-1520, 2008.
Kawaguchi Y, Kubota Y.GABAergic cell subtypes and their synaptic connections in rat frontal cortex. *Cereb Cortex* 7:476-486, 1997.
Kim MJ, Loucks RA, Palmer AL, Brown AC, Solomon KM, Marchante AN, Whalen PJ. The structural and functional connectivity of the amygdala: from normal emotion to pathological anxiety. *Behav Brain Res* 223:403– 410, 2011.
Kitajima T, Hara K. An integrated model for activity-dependent synaptic modifications. *Neural Networks* 10:413-421, 1997.
Komatsu Y. GABAB receptors, monoamine receptors, and postsynaptic inositol trisphosphate-induced Ca2+ release are involved in the induction of long-term potentiation at visual cortical inhibitory synapses. *J Neurosci* 16: 6342–6352, 1996.
Kroner S, Rosenkranz JA, Grace AA, Barrionuevo G. Dopamine modulates excitability of basolateral amygdala neurons in vitro. *J Neurophysiol* 93:1598-1610, 2005.
Laviolette SR, Lipski WJ, Grace AA. A subpopulation of neurons in the medial prefrontal cortex encodes emotional learning with burst and frequency codes through a dopamine D4 receptor-dependent basolateral amygdala input. *J Neurosci* 25:6066-6075, 2005.
Laurent V, Westbrook RF. Distinct contributions of the basolateral amygdala and the medial prefrontal cortex to learning and relearning extinction of context conditioned fear. *Learn Mem* 15:657-666, 2008.
Li G, Nair SS, Quirk GJ. A biologically realistic network model of acquisition and extinction of conditioned fear associations in lateral amygdala neurons. *J Neurophysiol* 101:1629-1646, 2009.
Li G, Amano T, Pare D, Nair SS. Impact of infralimbic inputs on intercalated amygdala neurons: a biophysical modeling study. *Learn Mem* 18:226-240, 2011.
Likhtik E, Pelletier JG, Popescu AT, Pare D. Prefrontal control of the amygdala. *J Neurosci* 25:7429-7437, 2005.
Linke R, Braune G, Schwegler H. Differential projection of the posterior paralaminar thalamic nuclei to the amygdaloid complex in the rat. *Exp Brain Res* 134:520-532, 2000.
Loretan K, Bissiere S, Lüthi A. Dopaminergic modulation of spontaneous inhibitory network activity in the lateral amygdala. *Neuropharmacology* 47:631-639, 2004.
Markram H, Lubke J, Frotscher M, Roth A, Sakmann B. Physiology and anatomy of synaptic connections between thick tufted pyramidal neurons in the developing rat neocortex. *J Physiol (Lond)* 500:409-440, 1997.
Martina M, Bergeron R. D1 and D4 dopaminergic receptor interplay mediates coincident G protein-independent and dependent regulation of glutamate NMDA receptors in the lateral amygdala. *J Neurochem* 106:2421–2435, 2008.
Mueller D, Porter JT, Quirk GJ. Noradrenergic signaling in infralimbic cortex increases cell excitability and strengthens memory for fear extinction. *J Neurosci* 28:369-375, 2008.
Muller JF, Mascagni F, McDonald AJ. Dopaminergic innervation of pyramidal cells in the rat basolateral amygdala. *Brain Struct Funct* 213:275-288, 2009.
Myers KM, Davis M. Mechanisms of fear extinction. *Mol Psychiatry* 12:120-150, 2007.
Orozco-Cabal, L, Pollandt S, Liu J, Vergara L, Shinnick-Gallagher P, Gallagher JP. A novel rat medial prefrontal cortical slice preparation to investigate synaptic transmission from amygdala to layer V prelimbic pyramidal neurons. *J Neurosci Methods* 151:148-158, 2006.
Pare D, Quirk GJ, LeDoux JE. New vistas on amygdala networks in conditioned fear. *J Neurophysiol* 92:1-9, 2004.

Pare D, Duvarci S. Amygdala microcircuits mediating fear expression and extinction. *Curr Opin Neurobiol* 4:717-723, 2012

Pitkanen A, Stefanacci L, Farb CR, Go GG, LeDoux JE, Amaral DG. Intrinsic connections of the rat amygdaloid complex: projections originating in the lateral nucleus. *J Comp Neurol* 356:288–310, 1995.

Popescu AT, Pare D. Synaptic interactions underlying synchronized inhibition in the basal amygdale: evidence for existence of two types projection cells. *J Neurophysiol* 105:687-696, 2010.

Quirk GJ, Repa JC, LeDoux JE. Fear conditioning enhances short latency auditory responses of lateral amygdala neurons: parallel recordings in the freely behaving rat. *Neuron* 15:1029-1039, 1995.

Quirk GJ, Armony JL, LeDoux JE. Fear conditioning enhances different temporal components of tone evoked spike trains in auditory cortex and lateral amygdala. *Neuron* 19:613-624, 1997.

Rodriguez-Romaguera J, Sotres-Bayon F, Mueller D, Quirk GJ. Systemic propranolol acts centrally to reduce conditioned fear in rats without impairing extinction. *Biol Psychiatry* 65:887- 892, 2009.

Rosenkranz JA, Grace AA. Cellular mechanisms of infralimbic and prelimbic prefrontal cortical inhibition and dopaminergic modulation of basolateral amygdala neurons in vivo. *J Neurosci* 22: 324-337, 2002.

Rotaru DC, Lewis DA, Gonzalez-Burgos G. (2007) Dopamine D1 receptor activation regulates sodium channel-dependent EPSP amplification in rat prefrontal cortex pyramidal neurons. *J Physiol* 581:981-1000, 2007.

Repa JC, Muller J, Apergis J, Desrochers TM, Zhou Y, LeDoux JE. Two different lateral amygdala cell populations contribute to the initiation and storage of memory. *Nat Neurosci* 4:724-731, 2001.

Sah P, Faber ES, Lopez de Armentia M, Power J. The amygdaloid complex: anatomy and physiology. *Phsiol Rev* 83:803-834, 2003.

Salzman CD, Fusi S. Emotion, cognition, and mental state representation in amygdala and prefrontal cortex. *Annu Rev Neurosci* 33:173–202, 2010.

Samson RD, Pare D. Activity-dependent synaptic plasticity in the central nucleus of the amygdala. *J Neurosci* 25:1847-1855, 2005.

Santana N, Bortolozzi A, Serrats J, Mengod G, Artigas F. Expression of serotonin1A and serotonin2A receptors in pyramidal and GABAergic neurons of the rat prefrontal cortex. *Cereb Cortex* 14:1100-1109, 2004.

Santana N, Mengod G, Artigas F. Quantitative analysis of the expression of dopamine D1 and D2 receptors in pyramidal and GABAergic neurons of the rat prefrontal cortex. *Cereb Cortex* 19:849-860, 2009.

Sara SJ. The locus coeruleus and noradrenergic modulation of cognition. *Nat Neurosci Rev* 10:211-223, 2009.

Seamans JK, Durstewitz D, Christie BR, Stevens CF, Sejnowski TJ. Dopamine D1/D5 receptor modulation of excitatory synaptic inputs to layer V prefrontal cortex neurons. *Proc Natl Aca Sci* 98:301-306, 2001.

Sidiropoulou K, Lu FM, Fowler MA, Xiao R, Phillips C, Ozkan ED, Zhu MX, White FJ, Cooper DC. Dopamine modulates an mGluR5-mediated depolarization underlying prefrontal persistent activity. *Nat Neurosci* 12:190-199, 2009.

Sierra-Mercado D, Padilla-Coreano N, Quirk GJ. Dissociable roles of prelimbic and infralimbic cortices, ventral hippocampus, and basolateral amygdala in the expression and extinction of conditioned fear. *Neuropsychopharmacology* 36:529-538, 2011.

Shouval HZ, Castellani GC, Blais BS, Yeung LC, Cooper LN. Converging evidence for a simplified biophysical model of synaptic plasticity. *Biol Cybern* 87:383-391, 2002a.

Shouval HZ, Bear MF, Cooper LN. A unified model of NMDA receptor-dependent bidirectional synaptic plasticity. *Proc Natl Aca Sci* 99:10831-10836, 2002b.
Sotres-Bayon F, Quirk GJ. Prefrontal control of fear: more than just extinction. *Curr Opin Neurobiol* 20:231–235, 2010.
Sotres-Bayon F, Sierra-Mercado D, Pardilla-Delgado N, Quirk GJ. Gating of fear in prelimbic cortex by hippocampal and amygdala inputs. *Neuron*, in press.
Spruston N, Jaffe DB, Johnston D. Dendritic attenuation of synaptic potentials and currents: the role of passive membrane properties. *Trends Neurosci* 17:161-166, 1994.
Stuart G, Spruston N. Determinants of voltage attenuation in neocortical pyramidal neuron dendrites. J Neurosci 18:3501-10, 1998.
Takahashi H, Takano H, Kodaka F, Arakawa R, Yamada M, Otsuka T, Hirano Y, Kikyo H, Okubo Y, Kato M, Obata T, Ito H, Suhara T. Contribution of dopamine D1 and D2 receptors to amygdala activity in human. *J Neurosci* 30:3043–3047, 2010.
Trantham-Davidson H, Neely LC, Lavin A, Seamans J. Mechanisms underlying differential D1 versus D2 dopamine receptor regulation of inhibition in prefrontal cortex. *J Neurosci* 24:10652-10659, 2004.
Tully K, Bolshakov VY. Emotional enhancement of memory: how norepinephrine enables synaptic plasticity. *Molecular Brain* 3:15, 2010.
Tunnanen J, Pitkanen A. Do seizures cause neuronal damage in rat amygdala kindling? *Epilepsy Res* 39:171-176, 2000.
Vertes RP. Differential projections of the infralimbic and prelimbic cortex in the rat. *Synapse* 51:32–58, 2004.
Vidal-Gonzalez I, Vidal-Gonzalez B, Rauch SL, Quirk GJ. Microstimulation reveals opposing influences of prelimbic and infralimbic cortex on the expression of conditioned fear. *Learn Mem* 13:728-733, 2006.
Wang J, Chen S, Nolan MF, Siegelbaum SA. Activity-dependent regulation of HCN pacemaker channels by cyclic AMP: signaling through dynamic allosteric coupling. *Neuron* 36:451- 461, 2002.
Wang M, Ramos BP, Paspalas CD, Shu Y, Simen A, Duque A, Vijayraghavan S, Brennan A, Dudley A, Nou E, Mazer JA, McCormick DA, Arnsten AF. α2A-Adrenoceptors strengthen working memory networks by inhibiting cAMP-HCN channel signaling in prefrontal cortex. *Cell* 129: 397–410, 2007.
Warman EN, Durand DM, Yuen GLF. Reconstruction of hippocampal CA1 pyramidal cell electrophysiology by computer simulation. *J Neurophysiol* 71: 2033–2045, 1994.
Washburn MS, Moises HC. Electrophysiological and morphological properties of rat basolateral amygdaloid neurons in vitro. *J Neurosci* 12: 4066–4079, 1992.
Woodruff AR, Sah P. Networks of parvalbumin-positive interneurons in the basolateral amygdala. *J Neurosci* 27:553-563, 2007.
Womble MD, Moises HC. Hyperpolarization-activated currents in neurons of the rat basolateral amygdala. *J Neurophysiol* 70: 2056-20605, 1993.
Yang CR, Seamans JK, Gorelova N. Electrophysiological and morphological properties of layers V-VI principal pyramidal cells in rat prefrontal cortex in vitro. *J Neurosci* 16: 1904–1921, 1996.
Zahm DS, Jensen SL, Williams ES, Martin JR. Direct comparison of projections from the central amygdaloid region and nucleus accumbens shell. Eur J Neurosci 11:1119-1126, 1999.

974 **TABLES**

975 Table 1. Numbers of model cells in the various regions.

Composition		
Structure	Biological #s of cells (Reference)	Model cells pyramids/interneurons
Prelimbic layer 2	64,000 (Gabbott et al. 2005)	320/80
Prelimbic layer 5	32,000 (Gabbott et al. 2005)	160/40
Basal amygdala	40,000 (Tuunanen and Pitkanen, 2000)	200/50

976

977 Table 2. Connectivity between different regions in the model.

Connectivity		
Connection	% presynaptic cells projecting with fanout in ()	Reference
PL 2-PL 2	All (4)	Fujisawa et al. (2008)
PL 2-PL 5	0%	Jones et al. (2005)
PL 5-PL 2	5% (4)	Jones et al. (2005), Fujisawa et al. (2008)
PL 5-PL 5	All (4)	Fujisawa et al. (2008)
BL-BL	All (4)	Tunnanen and Pitkanen (2000)
BL-PL 5	32% (5)	Likhtik et al. (2005)
BL-PL 2	32% (2)	Likhtik et al. (2005)
PL 2-BL	7-14% (2)	Likhtik et al. (2005)
LA-BL	All (20)	Tunnanen and Pitkanen (2000)

978

979 Table 3. Distribution of neuromodulator receptors in PL layers 2, 5 and BL.

PL		Principal cells/Interneurons	
		layer 2	layer 5
Dopamine	D_1	19%/28%	21%/30%
	D_2	4%/5%	19%/8%
Norepinephrine	α	48%/31%	47%/31%
	β	50%/31%	49%/33%
BL		Principal cells	
Dopamine	D_1	30%	
	D_2	30%	
Norepinephrine	α	45%	
	β	45%	

980

Table 4. Parametric studies related to the PL-BL connections.

4a. Varying number of presynaptic cells (with constant fan-out) in the two connections affected tone responses differentially.

Connectivity						
BL→PL	z-scores and #s: BL cells			z-scores and #s: PL cells		
	mean	s.e.m.	cells	mean	s.e.m.	cells
-10%	3.6	0.13	73	4.11	0.12	121
control	3.62	0.14	75	4.13	0.13	127
+10%	3.61	0.16	76	4.14	0.12	126
PL→BL	z-scores and #s: BL cells			z-scores and #s: PL cells		
	mean	s.e.m.	cells	mean	s.e.m.	cells
-10%	3.54	0.14	70	4.04	0.16	120
control	3.62	0.16	75	4.13	0.17	127
+10%	3.69	0.14	79	4.23	0.15	132

4b. Varying specific pre-synaptic cell types in each connection (keeping connectivity constant) also affected tone responses differentially.

Selective connectivity between BL (cells with NM-receptors and LA inputs) to PL (random cells)						
BL→PL	z-scores and #s: BL cells			z-scores and #s: PL cells		
	mean	s.e.m.	cells	mean	s.e.m.	cells
25%	3.8	0.13	72	4.17	0.14	125
50%	3.83	0.14	73	4.17	0.13	124
75%	3.86	0.15	75	4.19	0.15	126
100%	3.9	0.12	79	4.2	0.16	129
Selective connectivity between PL (cells with NM-receptors) to BL (random cells)						
PL→BL	z-scores and #s: BL cells			z-scores and #s: PL cells		
	mean	s.e.m.	cells	mean	s.e.m.	cells
25%	2.9	0.13	34	3.3	0.13	63
50%	3.3	0.12	52	3.6	0.17	89
75%	3.7	0.15	79	4.2	0.16	128
100%	3.9	0.15	83	4.4	0.13	136

Figure Titles

Figure 1. Structure of the LA-BL-PL network model with principal cells and local interneurons in PL, BL and LA regions. The PL network has two layers, 2 and 5. Layer 5 receives input from BL cells. PL cells in layer 2 project to BL. BL receives input from LA. The LA network receives tone and shock as the primary inputs.

Figure 2. Membrane potential responses of PL and BL model cells to intracellular current pulses. A: responses of intrinsic bursting PL cell to different current injections (60 pA, 100 pA and 120 pA; duration-1600 ms) were similar to those observed in vitro (Durstewitz et al. 2000). B: responses of BL type A cell to current injections (left: 300 pA; middle: 400 pA; right: -100 pA; duration 600 ms) were similar to those reported in Faber et al. (2001).

Figure 3. PL and BL cells exhibit sustained tone responses during conditioning. Panel (1) shows the spike train of a representative cell showing sustained responses during early extinction. Panel (2) is the peri-event time histogram (PETHs) showing the average z-scores (bin width, 3 s; tone duration 30 sec; z> 2.58 for > 3 bins) of LA, BL, and PL cells (LA: n=24; BL: n=75; PL : n=127) during different phases of fear training. Averages were taken over 2 trials for habituation (trials 4-5), conditioning (trials 4-5), early extinction (1-2) and late extinction (19-20). The triangle represents shock input during conditioning.

Figure 4. Effect of connectivity and neuromodulator manipulations on sustained tone responses in PL and BL. Average z-scores and spontaneous firing rates of PL (panel A; ANOVA with repeated measures: $F_{(4, 126)}=17.07$, $p< 0.001$) and BL (panel B ; ANOVA with repeated measures: $F_{(4, 74)}=13.45$, $p< 0.001$) during early extinction (trials 1-2) phase of fear training with different inactivation experiments . All tone responsive cells were included in the average (bin width 3 s; tone duration 30 sec; z> 2.58 for > 3 bins), and all bins except the first were used to discard transient LA activity. Ten bins prior to tone-onset were used to calculate z-scores. Grey line indicates the number of cells that satisfy z > 2.58 for three or more bins (axis on right side of figure). Spontaneous activity was calculated for all cells after conditioning during the 30 sec interval between conditioning and extinction phases. The following inactivation cases were considered: 1) LA inactivation; 2) BL inactivation; 3) PL inactivation; 4) with no neuromodulator release; and 5) selective inactivation of BL to PL connections with intact PL to BL connectivity.

Figure 5. Validation of model predictions by experiments. (A) Tone responses of PL cells with β-NE antagonist propranolol; (B) Tone responses of PL with BL inactivation. Average PETHs show the z-scores of tone responses (bin width- 3 s; tone duration-30 sec; control and NM antagonist; we picked 20 random PL cells from the ones that exhibited sustained tone responses in the model (N=127); average was taken over 2 trials during early extinction (1-2). Z-scores for each bin was calculated relative to pre-tone bins.

Figure 6. The model suggests that PL integrates convergent inputs from several sources such as LA, BL and VTA/LC to convert transient tone inputs from LA into sustained tone responses in PL. The two panels show the activity in the BL-PL network during (A) habituation, and (B) late conditioning and early extinction phases. Activity in Ce does not cross threshold during habituation and late extinction. But, during late conditioning and early extinction, Ce activity crosses threshold causing neuromodulator release into PL and BL. This increases activity in PL through the PL-BL-Ce circuit and causes further release of neuromodulators, thus sustaining PL tone responses. With the tone off, Ce activity gradually drops below threshold and stops neuromodulator release. LA activity is not potentiated during habituation and late extinction, and so cannot trigger neuromodulator release to sustain activity during these phases.

Figure A1. Neuromodulator release dynamics. We present a possible firing pattern of the cell representing Ce output, to illustrate how $NM(t)$ is calculated depending on the number of spikes per 200 ms interval. Neuromodulator concentration decays with time, and we used the function $NM(t) = NM(t_0) * e^{-\beta(t-t_0)}$ with $NM(t_0)$ incremented every 200 ms by the number of spikes exceeding the threshold of 2 spikes/ 200 ms, β = 10 ms^{-1}, with t_0 being the time when $NM(t_0)$ was last incremented. So, every 200 ms, $NM(t)$ is updated by adding the number of Ce spikes exceeding threshold, and this value is used as $NM(t_0)$ for the next 200 ms. If $NM(t)$ did not exceed the threshold, it continued to decay through the next time interval. $NM(t)$ was then normalized into the range 0-1 by dividing it by 5 which is the maximum value allowed for the variable $NM(t)$, and this normalized value was used to model neuromodulator release.

Figure A2. Model tone response of CeM output cell and associated concentration of neuromodulators. (Top) Peri-event time histogram (PETHs; bin-width 1 sec) showing the activity of CeM cell during late habituation (trials 4-5), conditioning, early extinction (extinction trials 1 and 2), and late extinction (trials 19 and 20). (Bottom) Normalized neuromodulator concentration, NM, during the different stages of the model protocol.

Figure A3. Comparison of the relative importance of the recurrent connections in the BL-PL network on the generation of sustained tone activity in the BL-PL network. Comparison of tone responses(bin width- 3 s; tone duration-30 sec) for three scenarios, a) Disabling all connectivity between BL and PL, b) Disabling connectivity from BL to PL only, and c) Disabling connectivity from PL to BL only.

APPENDIX

Mathematical Details.

The equation for each compartment (soma or dendrite) followed the Hodgkin-Huxley formulations (Byrne and Roberts 2004) in eqn. 1,

$$C_m dV_s/dt = -g_L(V_s - E_L) - g_c(V_s - V_d) - \sum I_{cur,s}^{int} - \sum I_{cur,s}^{syn} + I_{inj} \qquad (1)$$

where V_s/V_d are the somatic/dendritic membrane potential (mV), $I_{cur,s}^{int}$ and $I_{cur,s}^{syn}$ are the intrinsic and synaptic currents in the soma, I_{inj} is the electrode current applied to the soma, C_m is the membrane capacitance, g_L is the is the conductance of leak channel, and g_c is the coupling conductance between the soma and the dendrite (similar term added for other dendrites connected to the soma). The intrinsic current $I_{cur,s}^{int}$, was modeled as $I_{cur,s}^{int} = g_{cur} m^p h^q (V_s - E_{cur})$, where g_{cur} is its maximal conductance, *m* its activation variable (with exponent *p*), *h* its inactivation variable (with exponent *q*), and E_{cur} its reversal potential (a similar equation is used for the synaptic current $I_{cur,s}^{syn}$ but without *m* and *h*). The kinetic equation for each of the gating variables x (*m* or *h*) takes the form

$$\frac{dx}{dt} = \frac{x_\infty\left(V,[Ca^{2+}]_i\right) - x}{\tau_x(V,[Ca^{2+}]_i)} \qquad (2)$$

where x_∞ is the steady state gating voltage- and/or Ca^{2+}- dependent gating variable and τ_x is the voltage**-** and/or Ca^{2+}- dependent time constant. The equation for the dendrite follows the same format with '*s*' and '*d*' switching positions in eqn. 1. Details related to the model, including types of channels and parameter values are provided in table A1 for PL cells. Similar details for BL cells were from Li et al. (2009) and for Ce cells from Li et al. (2011), and so not repeated here.

Synaptic Currents

Excitatory transmission was mediated by AMPA/NMDA receptors, and inhibitory transmission by $GABA_A$ receptors. The corresponding synaptic currents (shown in dendrites below) were modeled by dual exponential functions (Durstewitz et al. 2000), as shown in eqns. 3-5,

$$I_{AMPA} = \bar{A} w(t) g_{AMPA,max} \frac{\tau_1\tau_2}{\tau_2-\tau_1}[\exp(-t/\tau_2) - \exp(-t/\tau_1)](V - E_{AMPA}) \qquad (3)$$

$$I_{NMDA} = \bar{A} w g_{NMDA,max} s(V) \frac{\tau_1\tau_2}{\tau_2-\tau_1}[\exp(-t/\tau_2) - \exp(-t/\tau_1)](V - E_{NMDA}) \qquad (4)$$

$$I_{CABA} = \bar{A} w(t) g_{GABAA,max} \frac{\tau_1\tau_2}{\tau_2-\tau_1}[\exp(-t/\tau_2) - \exp(-t/\tau_1)](V - E_{GABA}) \qquad (5)$$

where *V* is the membrane potential of the compartment (dendrite or soma) where the synapse is located, $w(t)$is the adjustable synaptic weight for AMPA synapses (see below; *w* was held fixed for all NMDA synapses); $\bar{A}$ is a normalization constant chosen so $g_{AMPA,max}$, $g_{NMDA,max}$ and $g_{GABA,max}$ assume maximum values of the conductances; τ_1 and τ_2 are the rise and decay time constants respectively. For AMPA receptor channels, τ_1 = 0.55 ms and τ_2 = 2.2 ms; for NMDA receptor channels, τ_1 = 10.7 ms and τ_2 = 125.0 ms, and for $GABA_A$ receptors, τ_1 = 0.25ms and τ_2 = 3.75 ms. The voltage-dependent variable *s*(*V*) which implements the Mg^{2+} block was defined as: $s(V) = [1 + 0.33\exp(-0.06\,V)]^{-1}$ (Zador et al., 1990). The maximal conductances were chosen as: $g_{AMPA,max}$= 1 nS, $g_{NMDA,max}$ = 0.5 nS and $g_{GABA,max}$= 0.6 nS. Synaptic reversal potentials were as follows: $E_{\mathrm{AMPA}} = E_{\mathrm{NMDA}} = 0$ mV and $E_{\mathrm{GABAA}} = -75$ mV (Durstewitz et al., 2000).

Calcium dynamics and Hebbian learning

Intracellular calcium was regulated by a simple first-order differential equation shown in Eqn. 6 (Warman et al. 1994; Li et al. 2009),

$$\frac{d[Ca^{2+}]_i}{dt} = -f\frac{I_{Ca}}{zFA} + \frac{[Ca^{2+}]_{rest} - [Ca^{2+}]_i}{\tau_{Ca}} \quad (6)$$

where *f* is the fraction of the Ca^{2+} influx (*f* =0.024), *V* = *wA* with *w* being the shell thickness (1μm) and *A* the dendritic/soma surface area, z=2 is the valance of the Ca^{2+} ion, *F* is the Faraday constant, and τ_{Ca} is the time constant associated with Ca^{2+} removal. The resting Ca^{2+} concentration was $[Ca^{2+}]_{rest}$ =50 nmol/l (Durstewitz et al. 2000).

A biophysical Hebbian rule (Gerstner and Kistler 2002; Shouval et al. 2002a,b; Li et al. 2009) was implemented by adjusting the synaptic weight $w(t)$ in synaptic conductances (Eqns. 3 and 5) using equation 7,

$$\Delta w_j = \eta([Ca^{2+}]_j)\Delta t(\lambda_1\Omega([Ca^{2+}]_j) - \lambda_2\omega_j) \quad (7)$$

where η is the Ca^{2+}-dependent learning rate and Ω is a Ca^{2+}-dependent function with two thresholds (θ_d and θ_p; $\theta_d \le \theta_p$) (for details see Li et al. 2009); λ_1 and λ_2 represent scaling and decay factors respectively; the local calcium level at synapse *j* is denoted by $[Ca^{2+}]_j$ and Δ*t* is the simulation time step. With this learning rule, the synaptic weight decreases when $\theta_d < [Ca^{2+}]_j < \theta_p$, and increases when $[Ca^{2+}]_j > \theta_p$, with modulation by the decay term $\lambda_2 w_j$.

Concentration of calcium pools: The concentration of the calcium pool at synapse *j* followed the dynamics in eqn. 6, with f_j=0.024 (Warman et al. 1994), $\tau_j = 50$ ms (Shouval et al. 2002b), *V* is the volume of a spine head with a diameter of $2\ \mu m$ (Kitajima and Hara 1997). All the synaptic weights were constrained by upper (W_{max}) and lower (W_{min}) limits (Li et al. 2009). Maximum (f_{max}) and minimum (f_{min}) folds were specified for each modifiable synapse so that $W_{max} = f_{max} * w(0)$ and $W_{min} = f_{min} * w(0)$.

Excitatory synapses onto principal cells. For tone-principal cell, and principal cell-principal cell connections, the calcium influx which determines learning was calculated by using the NMDA current, $I_{Ca}^N = P_0 w^{-1} G_{NMDA}(V - E_{Ca})$ (Shouval et al. 2002b), where G_{NMDA} = $\bar{A} w g_{NMDA,max} s(V) \frac{\tau_1\tau_2}{\tau_2-\tau_1}[\exp(-t/\tau_2) - \exp(-t/\tau_1)]$ from eqn. 4, the term w^{-1} ensures that it is calculated per synapse, and P_0 = 0.015.

Excitatory synapses onto interneurons. For tone-interneuron, and principal cell-interneuron connections, the calcium influx (used for learning) at the excitatory synapses on interneurons occurs through both NMDA and AMPA receptors (details in Li et al. 2009). In addition to calcium influx through NMDA current I_{Ca}^N, the calcium influx through AMPA receptors was calculated as $I_{Ca}^A = P_0 w^{-1}(0) G_{AMPA}(V - E_{Ca})$ where G_{AMPA} is the AMPA conductance in eqn. 4 (as described in the earlier para for G_{NMDA}), and *w*(0) is the initial AMPA synaptic weight, P_0 = 0.001. The Ca^{2+} current through the AMPA/NMDA receptors was separated from the total AMPA/NMDA current in this manner and used for implementation of the learning rule (Kitajima and Hara 1997; Li et al. 2009; Shouval et al. 2002a).

Inhibitory synapses onto principal cells. Several different mechanisms have been reported for potentiation at GABAergic synapses in other brain regions (e.g., Gaiarsa et al. 2002). A rise in postsynaptic intracellular Ca^{2+} concentration seems to be required in most mechanisms to trigger long-term plasticity. In the neonatal rat hippocampus, potentiation could be induced by Ca^{2+} influx through the voltage-dependent Ca^{2+} channels (VDCCs), whereas in the cortex and cerebellum, this process requires Ca^{2+} release from postsynaptic internal stores that is dependent on stimulation of GABA receptors (Gaiarsa et al. 2002). Thus, both presynaptic

activity (GABA receptor stimulation or interneuron firing) and postsynaptic activity (activation of VDCCs by membrane depolarization) contribute to the potentiation of GABA synapses. The process from GABA receptor stimulation to internal Ca^{2+} release involves activating a cascade of complex intracellular reactions (Komatsu 1996). Such a complex process can be simplified by assuming that the Ca^{2+} release is proportional to the stimulation frequency or $GABA_A$ conductance (Li et al. 2009). Hence we modeled this simplified process by considering Ca^{2+} release from the internal stores into a separate Ca^{2+} pool, using an equation similar to that for the AMPA/NMDA case cited above: $I_{Ca}^{G} = P_0 w^{-1}(t) G_{GABA}(V - E_{Ca})$ with P_0 = 0.01, and G_{GABA} as the $GABA_A$ conductance in eqn. 5 (as described earlier for G_{NMDA}). Note that the current I_{Ca}^{G}, models the dependence of Ca^{2+} release on $GABA_A$ stimulation frequency but not Ca^{2+} influx through the $GABA_A$ channel. The current I_{Ca}^{G}, together with post-synaptic voltage dependent calcium current (I_{Ca}), contributed towards plasticity. Hence, $I'_{Ca} = I_{Ca}^{G} + 0.01 I_{Ca}$ was used to calculate calcium influx for learning at such synapses (Li et al. 2009).

The initial weights and other learning parameters for the synapses are listed in table A2.

Neuromodulator release. Neuromodulator concentration decays with time, and we used the function $NM(t) = NM(t_0) * e^{-\beta (t - t_0)}$ with $NM(t_0)$ incremented every 200 ms by the number of Ce spikes exceeding the threshold of 2 spikes/ 200 ms, β=10 ms^{-1}, and t_0 the time when $NM(t_0)$ was last incremented (see Fig. A1). So, every 200 ms, $NM(t)$ is updated by adding the number of Ce spikes exceeding threshold (Fig. A2), and this value is used as $NM(t_0)$ for the following 200 ms period. If Ce output cell spikes did not exceed the threshold, $NM(t)$ continued to decay through the next time interval. Neuromodulator concentration decay was thus modeled similar to the decay of post-synaptic potentials, with Ce spikes mimicking synaptic input spikes. That is, Ce spikes above threshold 'summed' to increase concentration, much as synaptic spikes cause summation of post-synaptic potentials. $NM(t)$ was then normalized into the range 0 to 1using the maximum value (of 5) allowed for the variable $NM(t)$ in the model, and this normalized value was used to model neuromodulator effects in PL and BL. The NM_H and NM_L factors were determined as follows. $NM_L = NM(t)$, if $0 < NM(t) < NM\_bias$ (=0.2 in the model) for each 200 ms bin, else $NM_L = NM\_bias$. For high concentrations, $NM_H = NM(t) - NM\_bias$, if $NM(t) > NM\_bias$, for each 200 ms bin, else $NM_H = 0$. Existence of such a threshold in Ce was also hinted in a recent study (Amano et al. 2011) where inactivation of either the lateral (BL) or medial regions (BM) independently with muscimol did not cause a reduction of conditioned freezing, but inactivation of the entire basal amygdala (BL+BM) reduced conditioned freezing.

Table A1. Parameter values for PL single cell model.

A1a. Gating variables for ion channels

Current Type	Gating Variable	α	β	x_∞	τ_x (ms)
I_{Na}	$p = 3$	$\frac{-0.2816\,(V+28)}{\exp(-(V+28)/9.3)-1}$	$\frac{-0.2464\,(V+1)}{\exp((V+1)/6)-1}$	$\frac{\alpha}{\alpha+\beta}$	$\frac{1}{\alpha+\beta}$
	$q = 1$	$0.098 \times \exp(-(V+43.1)/20)$	$\frac{1.4}{\exp(-(V+13.1)/10)+1}$	$\frac{\alpha}{\alpha+\beta}$	$\frac{1}{\alpha+\beta}$
I_{NaP}	$p = 1$	$\frac{-0.2816\,(V+12)}{\exp(-(V+12)/9.3)-1}$	$\frac{-0.2464\,(V-15)}{\exp((V-15)/6)-1}$	$\frac{\alpha}{\alpha+\beta}$	$\frac{1}{\alpha+\beta}$
	$q = 1$	$2.8 \times 10^{-5} \times \exp(-(V+42.8477)/4.0248)$	$\frac{0.02}{\exp(-(V+413.93)/148.26)+1}$	$\frac{\alpha}{\alpha+\beta}$	$\frac{1}{\alpha+\beta}$
I_{DR}	$p = 4$	$\frac{-0.018(V-13)}{\exp(-(V-13)/25)-1}$	$\frac{0.0054\,(V-23)}{\exp(-(V-23)/12)-1}$	$\frac{\alpha}{\alpha+\beta}$	$\frac{1}{\alpha+\beta}$
I_{HVA}	$p = 2$	—	—	$\frac{1}{\exp(-(V+24.6)/11.3)+1}$	$1.25 \times sech\,(-0.031(V+37.1))$
	$q = 1$	—	—	$\frac{1}{\exp((V+12.6)/18.9)+1}$	420.0
I_D	$p = 1$	—	—	$\frac{1}{\exp(-(V+34)/6.5)+1}$	6.0
	$q = 1$	—	—	$\frac{1}{\exp((V+65)/6.6)+1}$	$200 + \frac{1}{\exp(-(V+63.6)/4)+}$
I_{KCa}	$p = 2$	$\frac{-0.00642V_m-0.1152}{\exp(-(V_m+18)/12)-1}$ With $V_m = V + 40\,log_{10}([Ca]_i)$	$1.7 \times \exp(-(V_m+152)/30)$	$\frac{\alpha}{\alpha+\beta}$	$\max\left(\frac{1}{\alpha+\beta}, 1.1\right)$
I_{KIR}	$p = 1$	—	—	$\frac{1}{\exp(-(V+111)/11)+1}$	1
I_{HCN}	O	$\frac{-0.0015}{\exp((V+135.7)/6.45)-1}$	$\frac{-0.02}{\exp(-(V+99.7)/6.94)-1}$		
	AO	$\frac{-0.0067}{\exp((V+142.28)/13.3)-1}$	$\frac{-0.014}{\exp(-(V+83.5)/6.94)-1}$		

A1b. Maximal conductance densities (in ms/cm^2) of ion channels.

Conductance		I_{Na}	I_{DR}	I_{NaP}	I_{HVA}	I_{KS}	I_{Ca}
PL	Soma	120	50	2	0.4	.08	2.1
	Dend	20	14	0.8	0.8	.08	2.1

Modeling HCN channels based on Wang et al., (2002)

The cyclic allosteric model for cAMP modulation of HCN gating. α_0 and β_0 are the first-order, voltage-dependent rate constants for activation and deactivation, respecetively of unliganded channels; α_A and β_A are the voltage-dependent rate constants for the liganded channels. K_c =(k_{bc}/k_{fc}) , k_{bc} and k_{fc} rates of cAMP unbinding and binding, respectively, to the closed channel. K_o =(k_{bo}/k_{fo}), kbo and kfo are respective rates for closed channel. K_c and K_o depend on cAMP, varying cAMP conectration changes AO which determines the conductance of HCn channels.

$g_{hcn} = g_{hcn,max}*(0 + AO*g_{ca})$

g_{ca}= relative conductance of the bound state

C + AC + AO + O = 1

$$\begin{array}{ccc} A + C & \underset{\beta_o}{\overset{\alpha_o}{\leftrightarrow}} & O + A \\ K_c \updownarrow & & \updownarrow K_o \\ AC & \underset{\beta_A}{\overset{\alpha_A}{\leftrightarrow}} & AO \end{array}$$

$\alpha_0 = \frac{-0.0015}{\exp((V+135.7)/6.45)-1}$	$\beta_0 = \frac{-0.02}{\exp(-(V+99.7)/6.94)-1}$
$\alpha_A = \frac{-0.0067}{\exp((V+142.28)/13.3)-1}$	$\beta_A = \frac{-0.014}{\exp(-(V+83.5)/6.94)-1}$

Table A2. Model parameters for network connections and inputs.

Connection	Initial Weight	f_max (f_min=0.8 for all)	Delay (Poisson distributed mean)	Learning factor		Ca^{2+} Threshold	
				scaling	Decay	Low	High
Tone to LA	5	3	30	15	0.001	0.50	0.65
Tone to Interneuron (LA)	4	3	30	1.5	0.002	0.40	0.5
Interneuron(LA) to LA	5	4	4	2	0.002	0.55	0.7
LA to Interneuron (LA)	1	3	4	2	0.001	0.50	0.6
LA to LA	1.5	3	6	2.5	0.001	0.50	0.6
LA to BL	9	3	20	10	0.001	0.35	0.45
BL to BL	2	3	6	2	0.001	0.35	0.40
PL layer 2 to BL	12	3	30	10	0.001	0.30	0.40
Interneuron (BL) to BL	4	3	4	2	0.001	0.55	0.70
BL to Interneuron (BL)	4	3	4	1	0.001	0.50	0.60
BL to PL layer 5	5	3	20	15	0.001	0.35	0.45
PL5 to PL5	2	3	4	2	0.001	0.50	0.60
PL5 to Interneuron(PL5)	5	3	3	1	0.001	0.50	0.60
Interneuron(PL5) to PL5	5	3	3	2	0.001	0.55	0.70
BL to PL layer 2	4	3	20	15	0.001	0.35	0.45
PL2 to PL2	2	3	4	2	0.001	0.50	0.60
PL2 Interneuron(PL2)	5	3	3	1	0.001	0.50	0.60
Interneuron(PL2) to PL2	5	3	3	2	0.001	0.55	0.70
PL5 to PL2	3	3	8	2	0.001	0.50	0.60
Tone to CeM	12	3	8	2	0.001	0.50	0.60
BL to CeM	7	3	3	2	0.001	0.50	0.60
CeM to (output) CeM	10	3	3	2	0.001	0.50	0.60
LA to CeL	7	3	4	2	0.001	0.50	0.60
CeL to CeL	5	3	4	2	0.001	0.50	0.60
CeL to CeM	10	3	4	2	0.001	0.50	0.60

Note: The non-plastic weight of shock inputs to LA cells was 40 (Li et al. 2009).

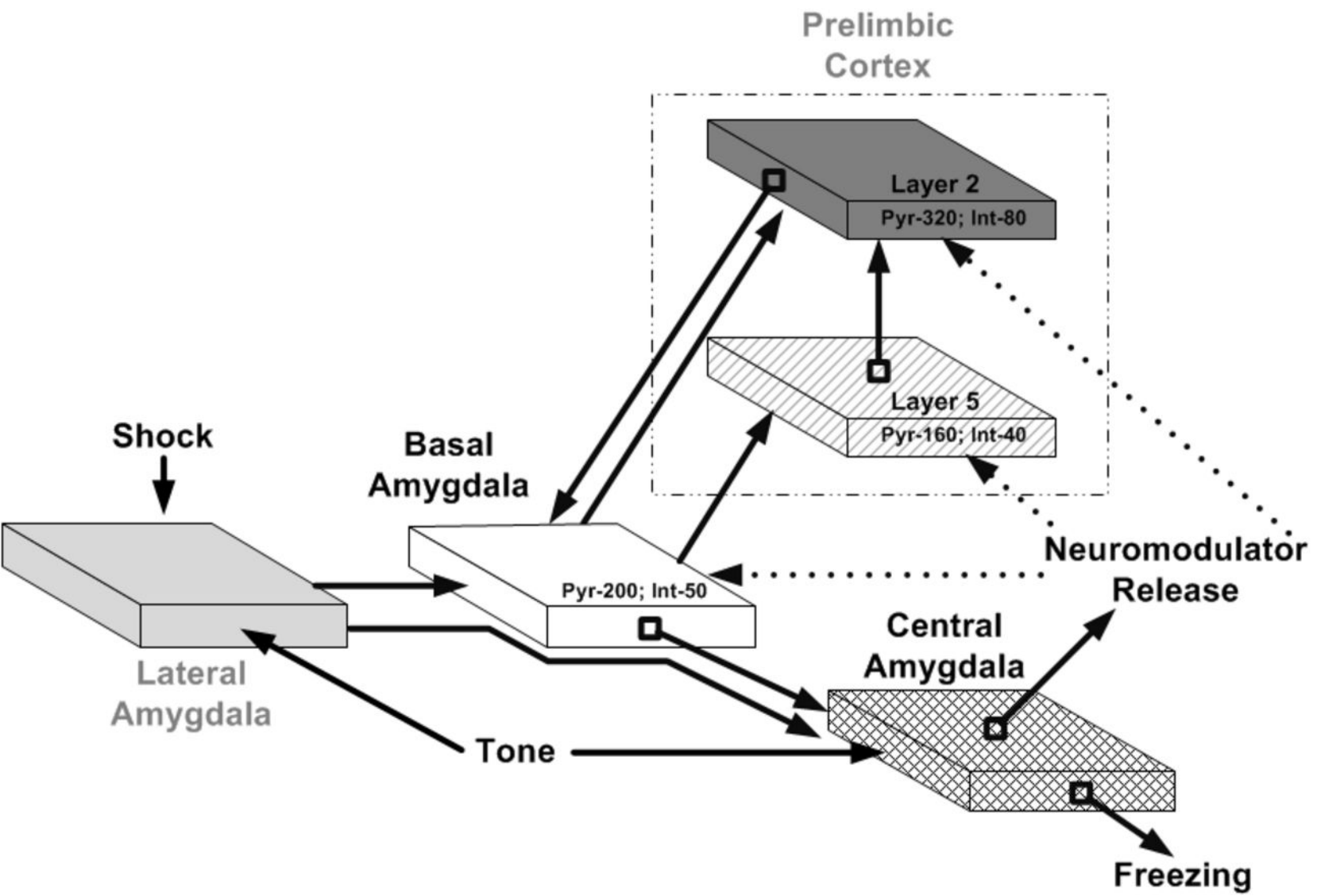
Prelimbic
Cortex
Layer 2
Pyr-320; Int-80
Layer 5
Pyr-160; Int-40
Shock
Basal
Amygdala
Pyr-200; Int-50
Neuromodulator
Release
Central
Amygdala
Lateral
Amygdala
Tone
Freezing

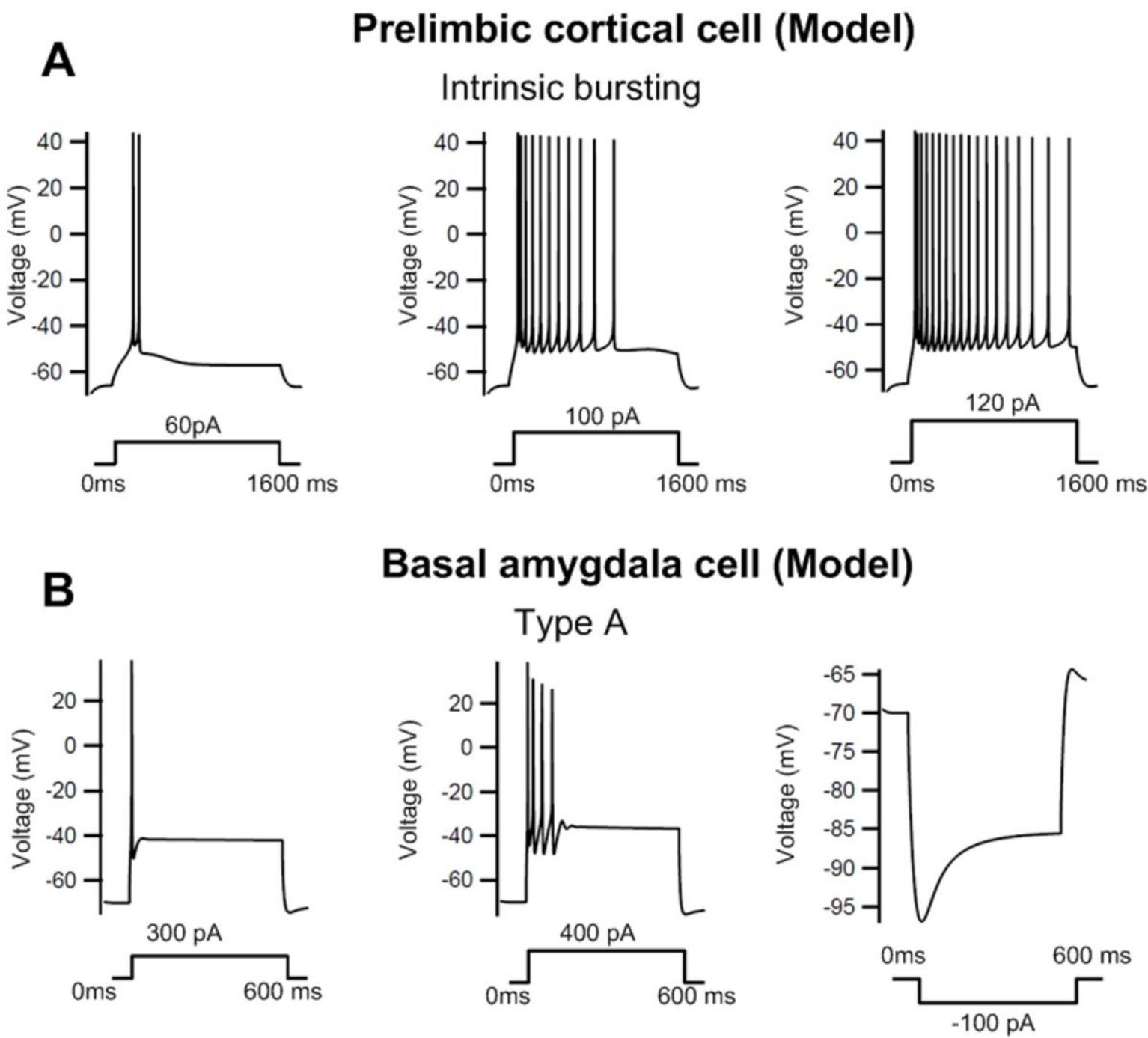
Prelimbic cortical cell (Model)
A
Intrinsic bursting
Voltage (mV)
40
20
0
-20
-40
-60
60pA
0ms
1600 ms
100 pA
120 pA
Basal amygdala cell (Model)
B
Type A
300 pA
400 pA
600 ms
-65
-70
-75
-80
-85
-90
-95
-100 pA

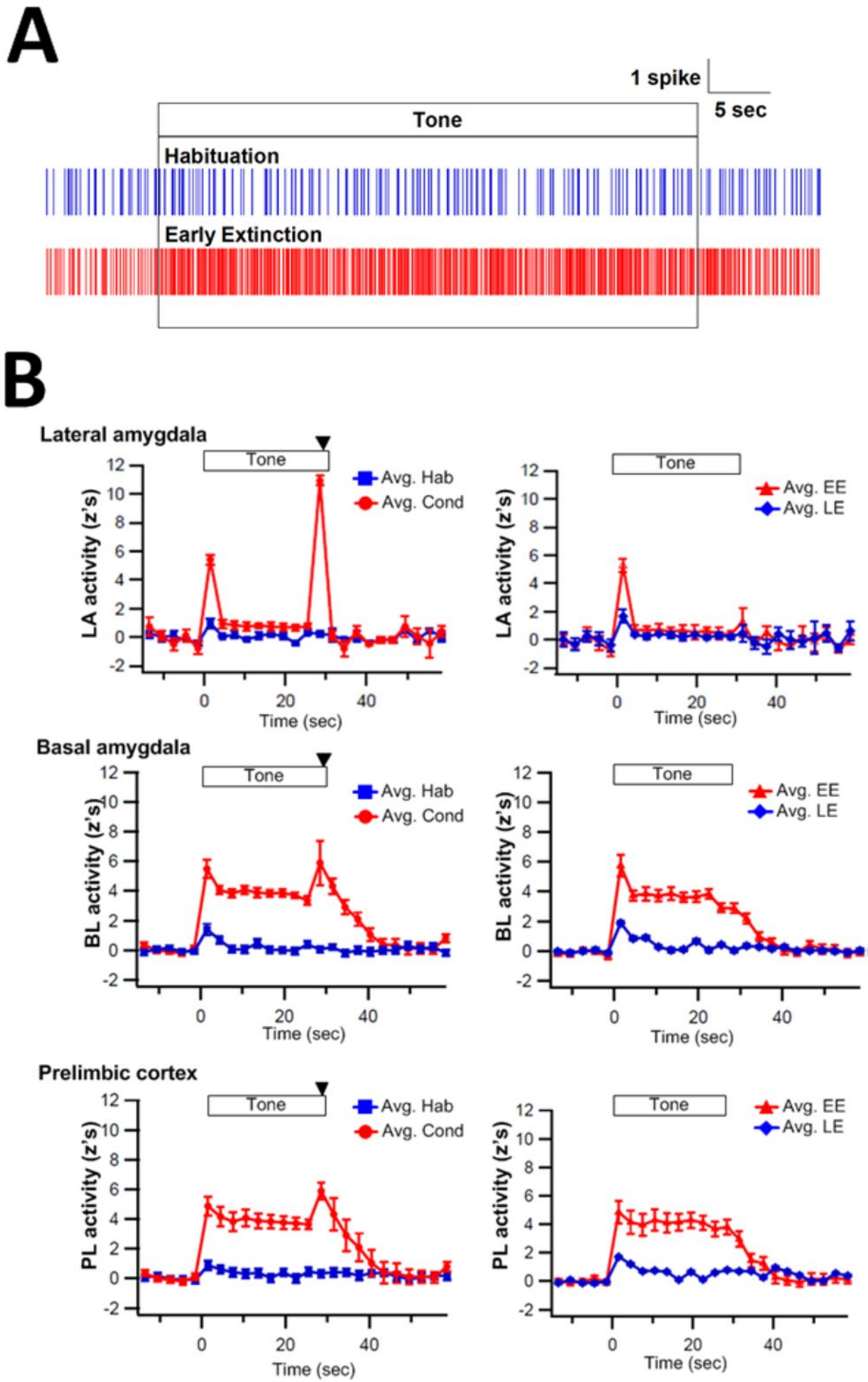
A
1 spike
5 sec
Tone
Habituation
Early Extinction
B
Lateral amygdala
Tone
Avg. Hab
Avg. Cond
LA activity (z's)
Time (sec)
Tone
Avg. EE
Avg. LE
LA activity (z's)
Time (sec)
Basal amygdala
Tone
Avg. Hab
Avg. Cond
BL activity (z's)
Time (sec)
Tone
Avg. EE
Avg. LE
BL activity (z's)
Time (sec)
Prelimbic cortex
Tone
Avg. Hab
Avg. Cond
PL activity (z's)
Time (sec)
Tone
Avg. EE
Avg. LE
PL activity (z's)
Time (sec)

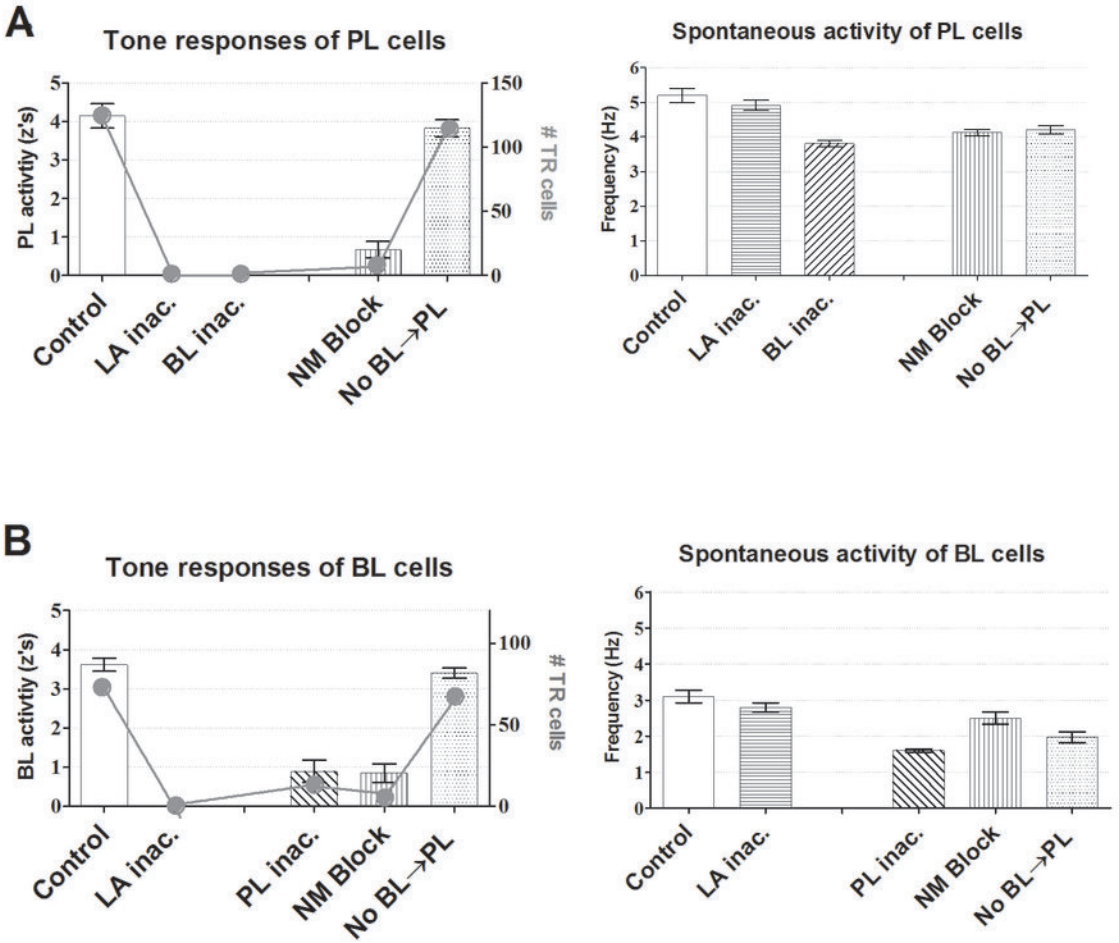
A
Tone responses of PL cells
PL activtiy (z's)
TR cells
Control
LA inac.
BL inac.
NM Block
No BL→PL
Spontaneous activity of PL cells
Frequency (Hz)
Control
LA inac.
BL inac.
NM Block
No BL→PL
B
Tone responses of BL cells
BL activtiy (z's)
TR cells
Control
LA inac.
PL inac.
NM Block
No BL→PL
Spontaneous activity of BL cells
Frequency (Hz)
Control
LA inac.
PL inac.
NM Block
No BL→PL

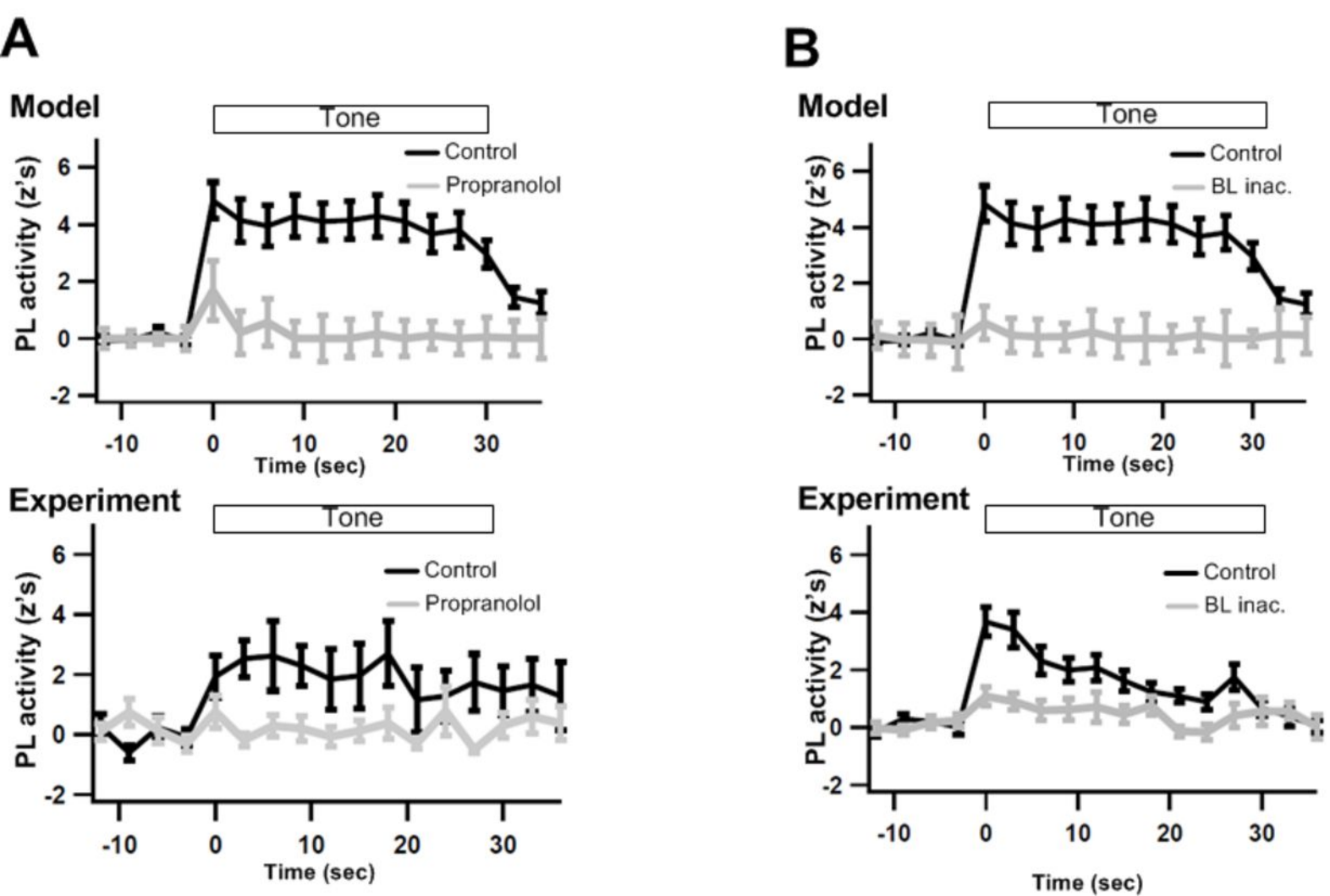
A
Model
Tone
Control
Propranolol
PL activity (z's)
6
4
2
0
-2
-10
0
10
20
30
Time (sec)
Experiment
Tone
Control
Propranolol
PL activity (z's)
6
4
2
0
-2
-10
0
10
20
30
Time (sec)
B
Model
Tone
Control
BL inac.
PL activity (z's)
6
4
2
0
-2
-10
0
10
20
30
Time (sec)
Experiment
Tone
Control
BL inac.
PL activity (z's)
6
4
2
0
-2
-10
0
10
20
30
Time (sec)

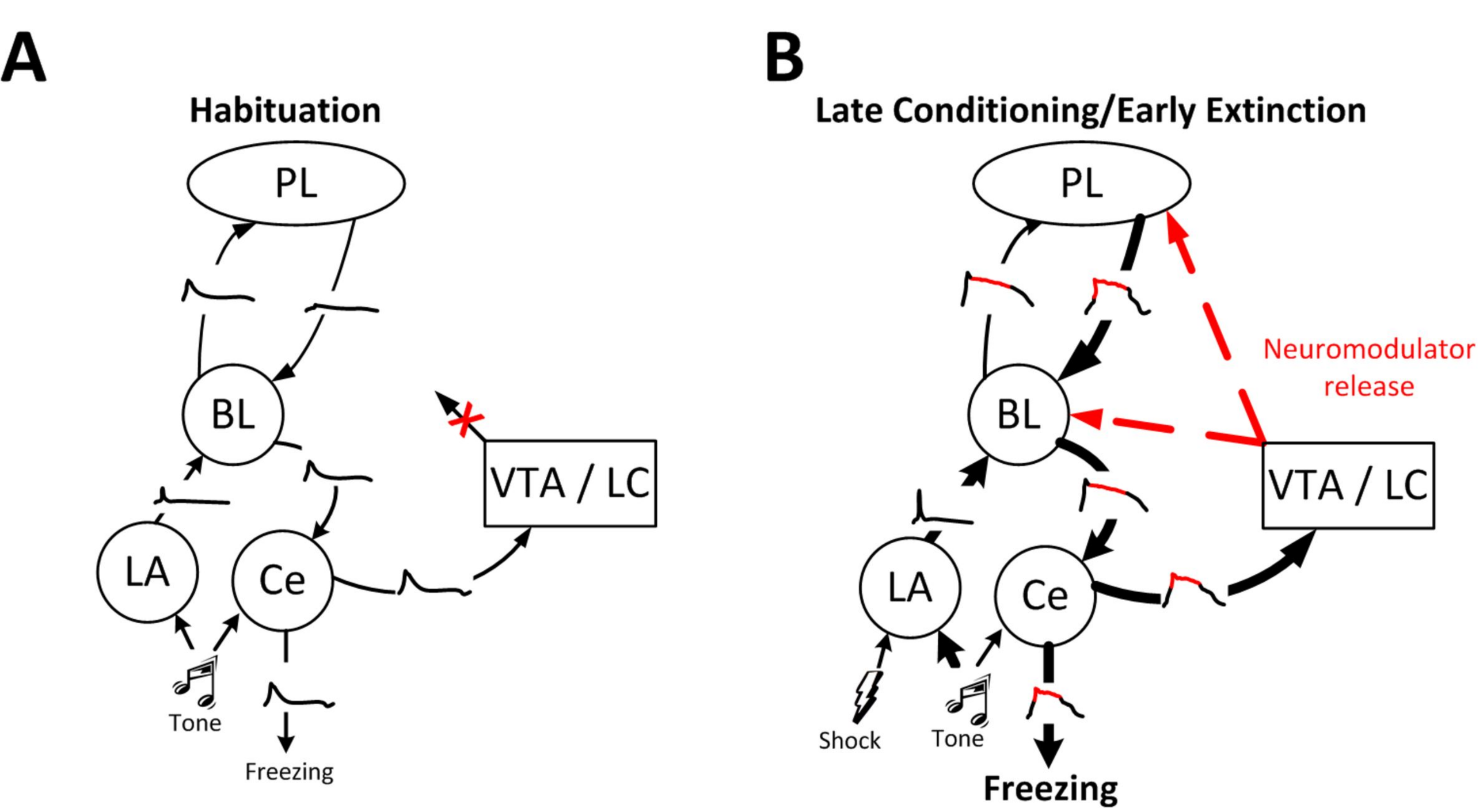
A
Habituation
PL
BL
LA
Ce
VTA / LC
Tone
Freezing
B
Late Conditioning/Early Extinction
PL
BL
LA
Ce
VTA / LC
Neuromodulator release
Shock
Tone
Freezing

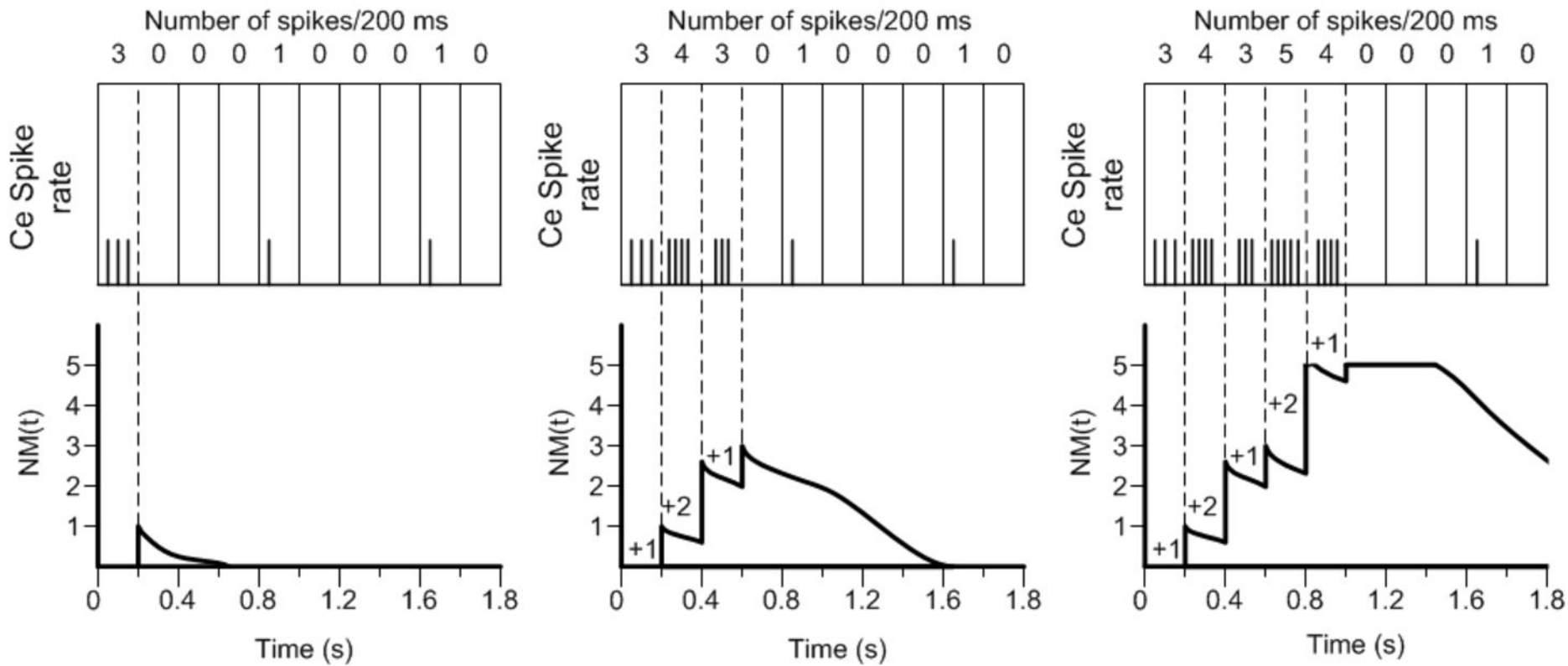
Number of spikes/200 ms
3 0 0 0 1 0 0 0 1 0
Ce Spike rate
NM(t)
5
4
3
2
1
0 0.4 0.8 1.2 1.6 1.8
Time (s)
Number of spikes/200 ms
3 4 3 0 1 0 0 0 1 0
Ce Spike rate
NM(t)
+1
+2
+1
Time (s)
Number of spikes/200 ms
3 4 3 5 4 0 0 0 1 0
Ce Spike rate
NM(t)
+1
+2
+1
+2
+1
Time (s)

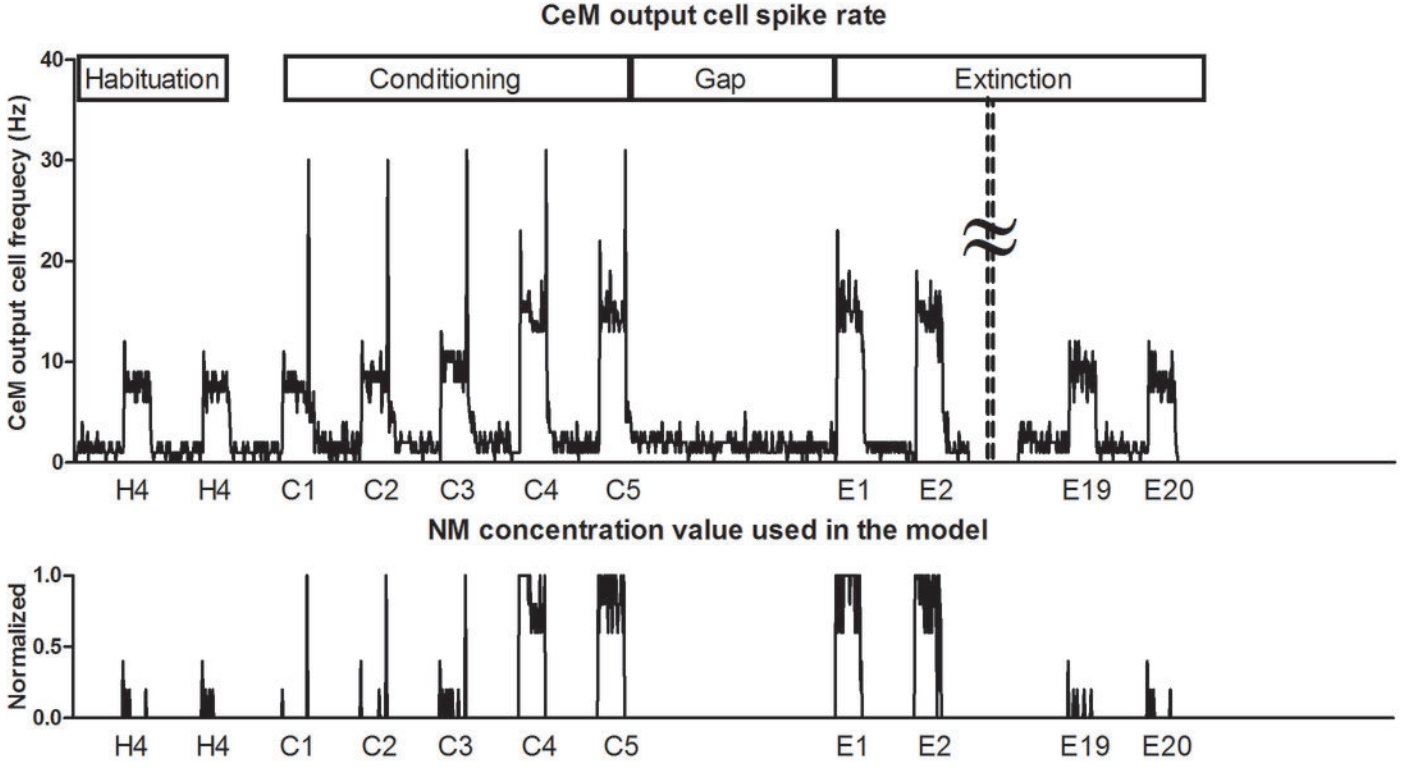
CeM output cell spike rate
Habituation
Conditioning
Gap
Extinction
CeM output cell frequecy (Hz)
40
30
20
10
0
H4
H4
C1
C2
C3
C4
C5
E1
E2
E19
E20
NM concentration value used in the model
Normalized
1.0
0.5
0.0
H4
H4
C1
C2
C3
C4
C5
E1
E2
E19
E20

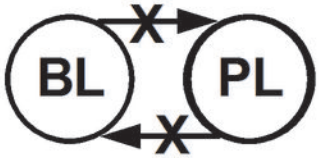

No BL ⇔ PL

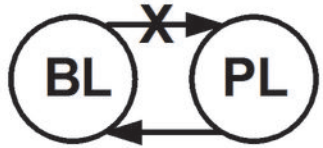

No BL ⇨ PL

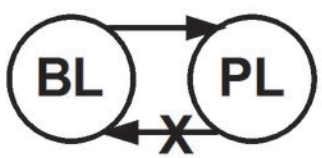

No PL ⇨ BL